Geophysical Journal International

Geophys. J. Int. (2012) **190,** 1640–1656 doi: 10.1111/j.1365-246X.2012.05566.x

An extension of the E/M_0 tsunami earthquake discriminant Θ to regional distances

Carl W. Ebeling and Emile A. Okal

Department of Earth and Planetary Sciences, Northwestern University, 1850 *Campus Drive, Evanston, IL* 60208, *USA.*
E-mails: carl@earth.northwestern.edu; emile@earth.northwestern.edu

Accepted 2012 June 7. Received 2012 June 6; in original form 2011 December 20

ABSTRACT

The 'slowness' parameter Θ, the logarithmic ratio of the estimated energy radiated by an earthquake E^{E} to its moment M_0, is a robust indicator of tsunami earthquakes when calculated from waveforms recorded at teleseismic epicentral distances ($35° < \Delta < 80°$). However, Θ values calculated from waveforms recorded at regional epicentral distances ($5° < \Delta < 35°$) are unreliable. This is because the necessary use of a differentiable traveltime $T(\Delta)$ curve smoothed through transition zone caustic distances leads to the systematic overestimation of E^{E}, and hence of Θ, for waveforms recorded at or near these distances. Using a data set comprised of 67 global oceanic dip-slip earthquakes occurring in the last 20 yr that includes six recognized tsunami earthquakes, we empirically develop a Θ correction for waveforms recorded at regional epicentral distances. Application of the correction to our data set allows the recovery of Θ values fully consistent with those calculated using only teleseismic waveforms. The incorporation of this correction into existing tsunami warning algorithms has the potential to significantly advance near-field warning efforts.

Key words: Tsunamis; Earthquake dynamics; Seismicity and tectonics; Body waves; Early warning.

1 INTRODUCTION

Our work here is motivated by the desire to more timely identify so-called 'tsunami earthquakes'. This has been a goal of the seismological and civil defence communities since 1972, when these exceptional earthquakes were recognized as a class distinct from 'typical' tsunamigenic earthquakes because they generate tsunamis greater than predicted by their conventional seismic magnitudes (Kanamori 1972). Tsunami earthquakes violate scaling laws (Geller 1976; Newman & Okal 1998), and are characterized by ruptures that are long (Kanamori 1972) and anomalously slow ($\sim$1 km s^{-1}; Kanamori 1972; Kikuchi & Kanamori 1995; Polet & Kanamori 2000). Because their sources release little high-frequency energy (Tanioka *et al.* 1997; Polet & Kanamori 2000), tsunami earthquakes provide a singular challenge to tsunami warning in general and to near-field self-evacuation in particular, since they may not be felt by people along coastlines most at risk.

The tsunami earthquake discriminant Θ introduced by Newman & Okal (1998) is a robust and quantitative estimator of such source high-frequency deficiency, when computed from waveforms recorded at teleseismic epicentral distances Δ between 35° and 80°. Newman & Okal (1998) impose these bounds on epicentral distance to avoid record contamination by later-arriving phases (such as *PcP*) at distances $\Delta > 80°$, and to avoid complexities related to triplications in the traveltime curve at distances $\Delta < 35°$.

The purpose of this paper is to investigate whether the effect of triplications can be overcome when waveforms recorded at regional epicentral distances ($5° < \Delta < 35°$) are used to calculate Θ. The incorporation of data recorded at these distances into Θ-processing algorithms will represent a significant advancement in near-field tsunami warning efforts.

1.1 The E/M_0 tsunami earthquake discriminant Θ

Boatwright & Choy's (1986) method to recover the total energy E^T radiated by a seismic source provides the foundation for Newman & Okal's (1998) energy-based tsunami earthquake discriminant Θ. Because their goal is a discriminant robust under real-time conditions (i.e. when source depth and focal geometry may not be known accurately), Newman & Okal (1998) adopt a default depth of $h =$ 15 km and a worldwide average anelastic attenuation operator, and assume average values for density and *P*-wave velocity at the source and receiver. An average distance-dependent focal correction F^{Est} replaces Boatwright & Choy's (1986) radiation coefficient F^{gP} for the generalized *P* wave (the combination of *P*, *pP* and *sP* phases). These factors and application of instrument response and receiver function corrections (Okal 1992) are incorporated in an estimated energy E^{E} algorithm (Newman & Okal 1998). Even though real scaled physical quantities are measured, Newman & Okal's (1998) approach thus retains the philosophy of a magnitude scale.

Newman & Okal (1998) define the 'slowness' parameter Θ as the logarithm of the dimensionless ratio of estimated radiated seismic energy E^E to seismic moment M_0:

$$\Theta = \log_{10}\left(\frac{E^E}{M_0}\right). \quad (1)$$

Observational Θ results of Newman & Okal (1998), based on waveforms from 52 large earthquakes recorded at teleseismic epicentral distances ($35° < \Delta < 80°$), are consistent with values predicted by scaling laws and the observations of Boatwright & Choy (1986). The one-to-one correspondence between values of Θ deficient by one logarithmic unit or more and the tsunami earthquakes of 1992 September 2 (Nicaragua), 1994 June 2 (Java) and 1996 February 21 (Peru) demonstrated by Newman & Okal (1998) holds for tsunami earthquakes taking place after their study.

The Pacific Tsunami Warning Center (PTWC), currently using only teleseismic waveforms, routinely calculates teleseismic Θ under operational conditions in real time. Values of the seismic moment M_0, necessary to compute Θ using eq. (1), can be obtained in quasi-real time by application of the *W*-phase inversion algorithm of Kanamori & Rivera (2008), or later from classical mantle Rayleigh waves using the M_m algorithm of Okal & Talandier (1989).

The PTWC determines Θ in overlapping time windows as introduced in Weinstein & Okal (2005) because it is stable over times comparable to source durations for true tsunami earthquakes, as opposed to events featuring delayed energy release (e.g. Peru, 2001 June 23). Earthquakes with Θ values more deficient than −5.8 receive special attention within PTWC operations (S. Weinstein, personal communication, 2012).

1.1.1 Thrust events recorded at regional distances

We recall that Newman & Okal (1998) suggested a possible systematic bias in estimated energy E^E for strike-slip earthquakes, since the majority of their teleseismic rays depart close to the null axis in the geometry of a perfect mechanism (which may in reality be slightly inaccurate or subject to lateral heterogeneity), thereby rendering excessive what should be a large focal mechanism correction. In the regional field, such an effect would be minimized because rays distance themselves from the null axis. This results in larger radiation patterns that are thus both closer to their average on the focal sphere and less sensitive to uncertainties in source and path. Since this topic remains controversial (Choy & McGarr 2002; Weinstein & Okal 2005), we take here a conservative approach and restrict our study to a robust data set, which excludes earthquakes with null axes plunging steeper than 50°. In practical terms, this has little effect in subduction zones, where strike-slip earthquakes are relatively rare.

2 DEVELOPMENT OF AN EMPIRICAL Θ CORRECTION FOR WAVEFORMS RECORDED AT REGIONAL DISTANCES

2.1 The effect of transition zone discontinuities on estimated energy E^E and Θ

Rays recorded at regional epicentral distances bottom in the transition zone and sample the 410 km and 660 km discontinuities. This leads to triplications in the traveltime curve $T(\Delta)$ and sharp reversals in the ray parameter (or slowness) curve $p(\Delta)$. The estimated energy E^E is inversely dependent upon geometrical spreading $g(\Delta)$ (Newman & Okal 1998), and therefore upon the second derivative of $T(\Delta)$ [or the first derivative of the $p(\Delta)$ curve]. E^E can thus be calculated only where this curve is differentiable, necessitating the use of a $T(\Delta)$ curve smoothed through caustic epicentral distances because $dp/d\Delta$ is discontinuous there. This in turn leads to systematic overestimation of E^E, and therefore of Θ, for waveforms recorded at and near caustic epicentral distances.

Distance ranges to triplications depend on tectonic environment (e.g. Burdick & Helmberger 1978; Given & Helmberger 1980; LeFevre & Helmberger 1989; Gaherty *et al.* 1999) and event depth, but in general, seismograms sample the 410 km discontinuity at distances between 15° and 25°, and the 660 km discontinuity between 20° and 30°. Caustics result at epicentral distances of about 15°, 20° and 25°.

Newman & Okal (1998) compute $g(\Delta)$ by direct numerical differentiation of $T(\Delta)$ using the Jeffreys–Bullen (JB) tables. At epicentral distances $\Delta > 35°$, this produces a smooth function $g(\Delta)$ robust with respect to varied traveltime tables. When extending this approach to regional distances ($\Delta < 35°$), the use of the JB tables is expected to misrepresent $g(\Delta)$ because the JB model does not include the 410 and 660 km discontinuities. Indeed, the use of traveltime curves based on any representative earth model requires smoothing to produce an acceptable differentiable function. Even though they have now been superseded by more sophisticated and realistic models, the JB tables nonetheless provide a zeroth-order model for the development of an adequate empirical distance correction. As shown in Fig. 1, the inverse geometrical spreading factor $1/g(\Delta)$, derived by double differentiation of the JB tables, still exhibits some oscillation at distances of interest here. This probably results from *ad hoc* interpolation through the transition zone used in table generation.

For any given waveform, we compute initial values of Θ using a simple numerical differentiation of the original JB tables. We call these Θ_{RU} (subscript 'U' denotes uncorrected and 'C' corrected) and Θ_T, when calculated from data recorded at regional and teleseismic distances, respectively. The ability of Θ_{RU} to replicate Θ_T will be assessed through statistical comparison of regional and teleseismic portions the Θ data set.

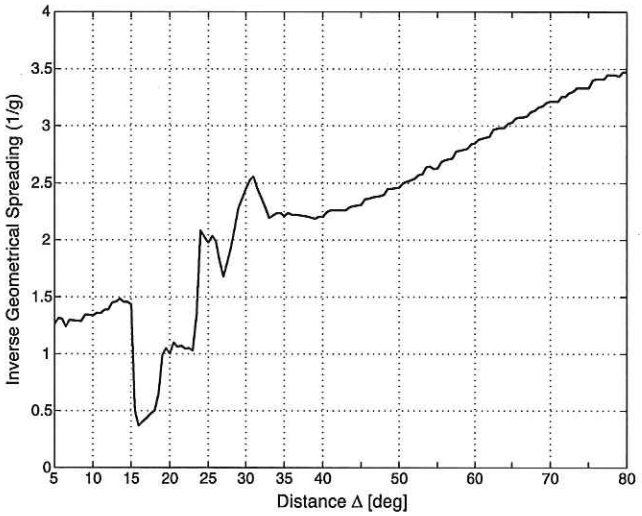

Figure 1. Inverse geometrical spreading $1/g(\Delta)$ based on Jeffreys–Bullen traveltime tables for regional ($5° < \Delta < 35°$) and teleseismic ($35° < \Delta < 80°$) epicentral distance ranges used in this study.

2.2 Correction development (comparison) data set

The data set used in correction development comprises waveforms from 67 earthquakes taking place during the last two decades (Table 1 and Fig. 2).

Our interest lies with the potential application of these results to tsunami warning. Thus all comparison earthquakes occurred in oceanic environments at subduction zones. Because their tsunami generation potential is greater, we further limit selection to events having focal geometries with null axes plunging less than 50° (the median null axis plunge for comparison events is 6°), and seismic moments $M_0 > 1.0 \times 10^{26}$ dyn cm ($M_w > 6.6$). The resulting data set of thrust- and normal-dominated earthquakes eliminates possible problems associated with strike-slip focal geometries.

Six known tsunami earthquakes, each highlighted in Table 1 and marked with stars in Fig. 2, are included in the comparison data set. Several large tsunamigenic earthquakes are also included, most notably the great $M_w = 8.8$ Maule, Chile event of 2010 February 27 (Event 63). The great $M_w = 9.1$ Tohoku, Japan, event of 2011 March 11 (Event V3) is one of 23 additional validation events purposely not included in the correction data set (see Section 3.3).

We used broad-band vertical (BHZ) waveforms obtained from the Incorporated Research Institutions for Seismology (IRIS) Data Management Center (DMC). Waveforms used in teleseismic Θ analysis were requested from only stations of the Global Seismic Network (GSN) located at epicentral distances $35° < \Delta < 80°$, while waveforms from any station meeting source–receiver distance requirements ($5° < \Delta < 35°$) were used in regional Θ analysis. Analysis in both cases was limited when possible to stations with a good signal-to-noise ratio.

We calculated Θ for each waveform with a fixed 70-s window beginning 5 s before the predicted *P*-wave arrival time using the algorithm of Newman & Okal (1998) and seismic moments from the Global Centroid-Moment-Tensor (CMT) Project catalogue (http://www.globalcmt.org/CMTsearch.html), generating a data set of 1520 regional and 1665 teleseismic event-station values (Θ_{RU} and Θ_T, respectively). CMT seismic moments were used because they provide continuity with the study of Newman & Okal (1998). Regional and teleseismic event-station values are plotted as a function of distance in Fig. 3(a). This distribution, shown as a histogram in Fig. 3(b), is characterized by a mean value $\overline{\Theta} = -5.04$ and a standard deviation $\sigma_\Theta = 0.77$.

We then compute event-averaged teleseismic $\overline{\Theta_T}$, the mean value of Θ_T over all stations for each event. We define the regional and

Table 1. Summary of all earthquakes used in this study with teleseismic (Θ_T) and regional uncorrected (Θ_{RU}) and corrected (Θ_{RC}) results with uncertainties of ±1 standard deviation. Comparison (oceanic) events numbered 1–67; validation events V1–V23; and continental earthquakes C1–C68. Only comparison (oceanic) earthquakes are used in development of regional Θ correction. Seismic moments M_0 are in units of 10^{27} dyn cm for comparison and validation events, and units of 10^{25} dyn cm for continental earthquakes. †: Tsunami earthquakes discussed in text and shown as stars in Fig. 2.

Event	Date (Julian day)	Time (UTC)	Epicentre (°N, °E)	Depth (km)	M_0	Foc. mech. ϕ, δ, λ (°)	Θ_T	Θ_{RU}	Θ_{RC}
1	1991 Apr 22 (112)	21:56	9.69, −83.07	10	3.3	103, 25, 58	−5.57 ± 0.41	−5.59 ± 0.50	−5.79 ± 0.30
†2	1992 Sep 02 (246)	00:16	11.74, −87.34	44	3.4	303, 12, 91	−6.47 ± 0.25	−6.44 ± 0.59	−6.70 ± 0.36
3	1992 Dec 12 (347)	05:29	−8.48, 121.90	27	5.1	80, 40, 95	−4.88 ± 0.38	−4.71 ± 0.39	−4.86 ± 0.24
4	1993 Jul 12 (193)	13:17	42.85, 139.20	16	4.7	0, 35, 91	−4.55 ± 0.29	−4.30 ± 0.55	−4.85 ± 0.26
5	1993 Aug 08 (220)	08:34	12.98, 144.80	59	5.2	312, 18, 147	−4.68 ± 0.26	−4.35 ± 0.53	−4.63 ± 0.40
†6	1994 Jun 02 (153)	18:17	−10.48, 112.83	18	5.3	278, 7, 89	−6.57 ± 0.40	−6.70 ± 0.39	−6.81 ± 0.32
7	1994 Oct 04 (277)	13:33	43.77, 147.32	14	30.0	158, 41, 24	−4.52 ± 0.41	−4.67 ± 0.43	−5.05 ± 0.38
8	1995 Jul 30 (211)	05:11	−23.34, −70.29	45	12.1	354, 22, 87	−5.41 ± 0.39	−5.41 ± 0.88	−5.87 ± 0.66
9	1995 Aug 16 (228)	10:27	−5.80, 154.18	30	4.6	136, 42, 87	−5.25 ± 0.37	−5.06 ± 0.87	−5.42 ± 0.66
10	1995 Oct 09 (282)	15:35	19.06, −104.21	33	11.5	302, 9, 92	−5.78 ± 0.24	−5.39 ± 0.59	−5.74 ± 0.44
11	1995 Dec 03 (337)	18:01	44.66, 149.30	33	8.2	225, 12, 95	−5.44 ± 0.43	−5.47 ± 0.60	−5.94 ± 0.54
12	1996 Jan 01 (001)	08:05	0.73, 119.93	24	7.8	36, 6, 54	−5.48 ± 0.34	−5.35 ± 0.47	−5.63 ± 0.38
13	1996 Feb 17 (048)	05:59	−0.89, 136.95	33	24.0	103, 11, 69	−5.74 ± 0.26	−5.35 ± 0.71	−5.73 ± 0.47
†14	1996 Feb 21 (052)	21:51	−9.59, −79.59	10	2.2	335, 14, 88	−6.06 ± 0.32	−5.67 ± 0.30	−5.90 ± 0.30
15	1996 Jun 10 (162)	04:03	51.56, −177.63	33	8.1	248, 17, 84	−5.49 ± 0.33	−5.08 ± 0.41	−5.24 ± 0.37
16	1996 Nov 12 (317)	16:59	−14.99, −75.68	33	4.6	312, 33, 55	−5.16 ± 0.33	−4.52 ± 0.53	−4.97 ± 0.37
17	1997 Dec 05 (339)	11:26	54.84, 162.04	33	5.3	202, 23, 4	−5.46 ± 0.37	−5.06 ± 0.62	−5.49 ± 0.40
18	1999 Sep 20 (263)	17:47	23.77, 120.98	33	3.4	37, 25, 96	−5.05 ± 0.32	−4.94 ± 0.61	−5.38 ± 0.50
19	1999 Nov 26 (330)	13:21	−16.42, 168.21	33	1.7	174, 30, 67	−4.88 ± 0.25	−4.78 ± 0.54	−5.21 ± 0.38
20	2000 Jun 14 (156)	16:28	−4.72, 102.09	33	7.5	92, 55, 152	−4.69 ± 0.35	−4.76 ± 0.34	−4.89 ± 0.44
21	2000 Nov 16 (321)	04:54	−3.98, 152.17	33	12.4	328, 43, 3	−5.57 ± 0.38	−5.14 ± 0.69	−5.57 ± 0.49
22	2000 Nov 16 (321)	07:42	−5.23, 153.10	30	6.5	253, 15, 93	−5.68 ± 0.46	−5.31 ± 0.94	−5.71 ± 0.66
23	2000 Nov 17 (322)	21:01	−5.50, 151.78	33	5.6	230, 24, 64	−6.11 ± 0.44	−5.72 ± 0.88	−6.12 ± 0.62
24	2001 Jan 13 (013)	17:33	13.05, −88.66	60	4.6	121, 35, −95	−4.85 ± 0.53	−4.99 ± 0.40	−5.07 ± 0.31
25	2001 Jun 23 (174)	20:33	−16.26, −73.64	33	47.0	310, 18, 63	−6.22 ± 0.56	−5.81 ± 0.66	−6.15 ± 0.53
26	2002 Mar 05 (064)	21:16	6.03, 124.25	31	1.9	314, 25, 70	−5.21 ± 0.32	−5.17 ± 0.55	−5.55 ± 0.54
27	2003 May 21 (141)	18:44	36.96, 3.63	12	0.2	57, 44, 71	−4.56 ± 0.29	−4.52 ± 0.48	−4.97 ± 0.43
28	2003 Aug 21 (233)	12:12	−45.10, 167.14	28	0.8	35, 23, 95	−4.81 ± 0.35	−4.53 ± 0.54	−4.91 ± 0.21
29	2003 Sep 25 (268)	19:50	41.81, 143.91	27	30.0	250, 11, 132	−5.36 ± 0.37	−5.14 ± 0.66	−5.56 ± 0.57
30	2003 Nov 17 (321)	06:43	51.15, 178.65	33	5.3	280, 19, 122	−5.51 ± 0.56	−5.26 ± 0.62	−5.68 ± 0.46
31	2004 Oct 09 (283)	21:26	11.42, −86.67	35	0.3	311, 26, 98	−5.26 ± 0.56	−4.72 ± 0.66	−4.90 ± 0.59
†32	2004 Dec 26 (361)	00:58	3.30, 95.98	30	1000	329, 8, 110	−6.91 ± 0.37	−6.82 ± 0.41	−6.92 ± 0.40
33	2005 Mar 28 (087)	16:09	2.09, 97.11	30	100	333, 8, 118	−5.54 ± 0.39	−5.43 ± 0.38	−5.61 ± 0.30

Table 1. *(Continued.)*

Event	Date (Julian day)	Time (UTC)	Epicentre (°N, °E)	Depth (km)	M_0	Foc. mech. ϕ, δ, λ (°)	Θ_T	Θ_{RU}	Θ_{RC}
34	2005 Nov 14 (318)	21:38	38.11, 144.90	11	0.4	181, 43, −104	−4.53 ± 0.33	−4.22 ± 0.46	−4.66 ± 0.39
35	2006 Apr 20 (110)	23:25	60.95, 167.09	22	3.1	207, 40, 76	−5.22 ± 0.24	−4.64 ± 0.51	−5.08 ± 0.36
36	2006 May 03 (123)	15:26	−20.19, −174.12	55	9.6	226, 22, 123	−4.35 ± 0.29	−4.26 ± 0.85	−4.75 ± 0.54
†37	2006 Jul 17 (198)	08:19	−9.25, 107.41	34	4.0	290, 10, 102	−5.94 ± 0.34	−6.04 ± 0.82	−6.38 ± 0.74
38	2006 Sep 28 (271)	06:22	−16.59, −172.03	28	0.3	6, 40, −100	−4.39 ± 0.56	−4.54 ± 0.43	−4.91 ± 0.22
39	2006 Oct 15 (288)	17:07	19.88, −155.93	38	0.1	88, 45, −146	−4.75 ± 0.41	−4.63 ± 0.28	−4.65 ± 0.29
40	2006 Nov 15 (319)	11:14	46.59, 153.27	10	33.7	215, 15, 92	−6.22 ± 0.34	−6.00 ± 0.63	−6.25 ± 0.42
41	2006 Dec 26 (360)	12:26	21.80, 120.55	10	0.3	165, 30, −76	−4.63 ± 0.26	−4.42 ± 0.42	−4.79 ± 0.30
42	2007 Jan 13 (013)	04:23	46.24, 154.52	10	16.5	266, 39, −54	−4.76 ± 0.44	−4.74 ± 0.65	−5.02 ± 0.53
43	2007 Jan 21 (021)	11:27	1.07, 126.28	22	2.0	34, 35, 108	−4.82 ± 0.36	−4.77 ± 0.45	−5.07 ± 0.40
44	2007 Apr 01 (091)	20:39	−5.80, 154.18	30	16.0	333, 37, 121	−5.35 ± 0.21	−5.30 ± 0.60	−5.47 ± 0.55
45	2007 Aug 15 (227)	23:40	−13.36, −76.52	30	11.1	321, 28, 63	−5.41 ± 0.43	−5.32 ± 0.65	−5.45 ± 0.64
46	2007 Sep 12 (255)	11:10	−4.37, 101.56	16	50.5	328, 9, 114	−5.35 ± 0.42	−4.92 ± 0.86	−5.34 ± 0.71
47	2007 Sep 12 (255)	23:49	−2.50, 100.15	44	7.8	317, 19, 102	−4.97 ± 0.38	−4.60 ± 0.70	−4.86 ± 0.52
48	2007 Sep 13 (256)	03:35	−2.22, 99.56	10	0.4	312, 10, 90	−4.85 ± 0.40	−4.41 ± 0.74	−4.71 ± 0.59
49	2007 Sep 30 (273)	05:23	−49.42, 163.95	10	1.5	29, 36, 123	−4.79 ± 0.14	−4.65 ± 0.65	−5.05 ± 0.62
50	2007 Nov 14 (318)	15:41	−22.64, −70.62	38	4.8	358, 20, 98	−4.99 ± 0.32	−4.62 ± 0.77	−5.07 ± 0.45
51	2007 Dec 19 (353)	09:30	51.02, −179.27	28	0.7	274, 21, 118	−5.25 ± 0.22	−4.68 ± 0.77	−5.19 ± 0.56
52	2008 Oct 19 (293)	05:10	−21.82, −173.56	43	0.3	189, 44, 81	−4.41 ± 0.35	−4.59 ± 0.67	−4.89 ± 0.46
53	2008 Nov 16 (321)	17:02	1.50, 122.05	29	1.2	92, 20, 84	−5.09 ± 0.32	−4.50 ± 0.54	−4.83 ± 0.44
54	2009 Jan 03 (003)	19:44	−0.38, 132.83	15	3.4	99, 23, 47	−5.08 ± 0.27	−4.53 ± 0.69	−4.75 ± 0.55
55	2009 Jan 03 (003)	22:33	−0.58, 133.48	18	1.4	101, 26, 72	−4.80 ± 0.25	−4.46 ± 0.67	−4.68 ± 0.54
56	2009 Mar 19 (078)	18:17	−23.08, −174.23	49	4.0	205, 44, 98	−4.47 ± 0.23	−4.05 ± 0.72	−4.43 ± 0.60
57	2009 Jul 15 (196)	09:22	−45.85, 166.26	24	6.0	25, 26, 138	−5.33 ± 0.33	−5.06 ± 0.49	−5.26 ± 0.43
58	2009 Aug 10 (222)	19:56	14.16, 92.94	22	2.1	39, 36, −92	−4.72 ± 0.33	−4.78 ± 0.22	−4.83 ± 0.22
59	2009 Sep 02 (245)	07:55	−29.24, 107.33	53	0.6	54, 46, 117	−4.43 ± 0.34	−4.53 ± 0.05	−4.85 ± 0.05
60	2009 Sep 29 (272)	17:48	−15.13, −171.97	12	12.0	119, 38, −131	−4.83 ± 0.26	−3.87 ± 0.51	−4.29 ± 0.38
61	2009 Sep 30 (273)	10:16	−0.79, 99.67	78	2.7	74, 52, 139	−4.65 ± 0.36	−4.62 ± 0.49	−4.69 ± 0.64
62	2010 Jan 03 (003)	22:36	−8.88, 157.21	12	0.5	321, 21, 102	−5.18 ± 0.35	−4.26 ± 0.15	−4.84 ± 0.18
63	2010 Feb 27 (058)	06:35	−35.98, −73.15	23	184	19, 18, 116	−5.35 ± 0.46	−4.67 ± 0.61	−5.16 ± 0.57
†64	2010 Oct 25 (298)	14:42	−3.68, 99.29	12	6.7	316, 8, 96	−6.22 ± 0.29	−5.46 ± 0.59	−5.78 ± 0.46
65	2010 Dec 21 (355)	17:19	27.06, 143.73	19	1.4	110, 40, −137	−4.30 ± 0.29	−3.76 ± 0.56	−4.13 ± 0.41
66	2011 Jan 02 (002)	20:20	−38.71, −73.93	20	0.6	5, 13, 97	−5.18 ± 0.34	−4.72 ± 0.63	−4.95 ± 0.64
67	2011 Jan 13 (013)	16:16	−20.60, 168.33	13	0.4	341, 38, −80	−4.26 ± 0.20	−4.36 ± 0.53	−4.55 ± 0.37
V1	2011 Feb 11 (042)	20:05	−36.63, −73.56	18	0.2	15, 13, 104	−5.30 ± 0.42	−4.70 ± 0.60	−5.20 ± 0.54
V2	2011 Mar 09 (068)	02:45	38.56, 142.78	14	1.2	189, 12, 78	−5.18 ± 0.47	−4.55 ± 0.66	−4.99 ± 0.46
V3	2011 Mar 11 (070)	05:47	37.52, 143.05	20	531	203, 10, 88	−5.59 ± 0.45	−5.21 ± 0.46	−5.50 ± 0.40
V4	2011 Apr 03 (093)	20:06	−10.06, 107.72	19	0.2	98, 40, −112	−4.94 ± 0.28	−4.78 ± 0.32	−4.99 ± 0.19
V5	2011 Apr 07 (097)	13:11	17.34, −94.13	154	0.1	194, 32, −27	−5.44 ± 0.32	−4.82 ± 0.57	−5.17 ± 0.48
V6	2011 Apr 23 (113)	04:17	−10.47, 161.32	77	0.2	164, 47, 172	−4.66 ± 0.33	−4.36 ± 0.35	−4.51 ± 0.28
V7	2011 May 10 (130)	08:55	−20.29, 168.15	18	0.2	354, 42, −74	−4.25 ± 0.22	−4.47 ± 0.32	−4.54 ± 0.20
V8	2011 Jun 24 (175)	03:09	52.09, −171.77	74	1.0	15, 10, −160	−4.51 ± 0.30	−4.34 ± 0.55	−4.49 ± 0.41
V9	2011 Jul 06 (187)	19:03	−29.22, −175.83	22	3.0	163, 36, −114	−4.74 ± 0.34	−4.42 ± 0.79	−4.64 ± 0.67
V10	2011 Jul 29 (210)	07:42	−23.78, 179.92	539	0.2	100, 33, 120	−5.22 ± 0.51	−5.37 ± 0.82	−5.60 ± 0.67
V11	2011 Aug 20 (232)	16:55	−18.52, 167.94	34	0.6	342, 29, 93	−5.22 ± 0.21	−4.85 ± 0.66	−5.07 ± 0.45
V12	2011 Aug 30 (242)	06:57	−6.47, 126.68	469	0.3	352, 9, −113	−5.32 ± 0.48	−4.71 ± 0.68	−5.03 ± 0.64
V13	2011 Sep 02 (245)	10:55	51.96, −171.49	40	0.2	130, 39, 28	−5.21 ± 0.30	−4.70 ± 0.68	−4.84 ± 0.71
V14	2011 Sep 05 (248)	17:55	2.89, 97.84	94	0.1	102, 12, −128	−4.91 ± 0.31	−4.41 ± 0.83	−4.64 ± 0.63
V15	2011 Sep 15 (258)	19:31	−21.57, −179.17	630	1.2	311, 37, −7	−5.06 ± 0.53	−4.78 ± 0.59	−5.02 ± 0.50
V16	2011 Sep 16 (259)	19:26	40.22, 143.23	20	0.2	185, 13, 73	−5.17 ± 0.32	−4.79 ± 0.73	−5.27 ± 0.59
V17	2011 Oct 21 (294)	17:57	−28.79, −175.76	49	1.5	203, 38, 82	−4.66 ± 0.26	−4.48 ± 0.91	−4.71 ± 0.76
V18	2011 Oct 28 (301)	18:54	−14.52, −76.16	26	0.3	327, 16, 70	−4.95 ± 0.32	−4.57 ± 0.48	−4.68 ± 0.36
V19	2011 Nov 08 (312)	02:59	27.14, 125.81	231	0.3	155, 38, −117	−4.84 ± 0.29	−4.45 ± 0.64	−4.83 ± 0.53
V20	2011 Dec 14 (348)	05:05	−7.42, 146.86	348	0.5	68, 23, −6	−5.00 ± 0.52	−4.31 ± 0.63	−4.62 ± 0.68
V21	2012 Jan 01 (001)	05:28	31.60, 138.24	354	0.2	116, 18, −160	−5.27 ± 0.58	−4.66 ± 0.67	−5.02 ± 0.58
V22	2012 Feb 02 (033)	13:34	−17.65, 167.12	19	0.5	53, 52, −41	−4.82 ± 0.24	−4.87 ± 0.50	−5.02 ± 0.29
V23	2012 Feb 06 (037)	03:49	10.03, 123.28	12	0.1	31, 44, 99	−4.77 ± 0.32	−4.52 ± 0.81	−4.94 ± 0.75
C1	1996 Feb 03 (034)	11:14	27.15, 100.28	15	9.9	0, 36, −68	−4.92 ± 0.28	−4.32 ± 0.62	−4.82 ± 0.44
C2	1996 Nov 19 (324)	10:44	35.45, 77.86	15	24	180, 71, 170	−5.43 ± 0.42	−4.21 ± 0.85	−4.75 ± 0.59
C3	1997 Feb 04 (035)	10:37	37.82, 57.50	15	6.7	328, 81, −171	−5.19 ± 0.41	−4.47 ± 0.66	−4.84 ± 0.59
C4	1997 Feb 27 (058)	21:08	29.74, 68.13	15	52	298, 15, 122	−5.21 ± 0.32	−4.68 ± 0.53	−5.08 ± 0.40
C5	1997 May 10 (130)	07:57	33.58, 60.02	15	74	248, 83, 0	−5.27 ± 0.20	−4.38 ± 0.54	−4.69 ± 0.48

Table 1. *(Continued.)*

Event	Date (Julian day)	Time (UTC)	Epicentre (°N, °E)	Depth (km)	M_0	Foc. mech. ϕ, δ, λ (°)	Θ_T	Θ_{RU}	Θ_{RC}
C6	1997 May 13 (133)	14:13	36.51, 70.68	189	5.0	273, 38, 124	−4.67 ± 0.27	−3.96 ± 0.85	−4.26 ± 0.70
C7	1997 Nov 08 (312)	10:03	35.33, 86.96	16	223	79, 69, 2	−5.81 ± 0.32	−4.55 ± 0.76	−5.05 ± 0.51
C8	1998 Feb 20 (051)	12:18	36.50, 70.88	244	4.0	184, 15, 100	−4.92 ± 0.39	−4.52 ± 0.52	−4.77 ± 0.41
C9	1998 Mar 14 (073)	19:40	29.95, 57.60	15	9.4	154, 57, −174	−5.24 ± 0.29	−4.47 ± 0.53	−4.93 ± 0.47
C10	1998 May 30 (150)	06:22	37.38, 70.08	24	7.9	200, 79, −7	−5.37 ± 0.27	−4.66 ± 0.69	−5.02 ± 0.42
C11	1998 Aug 27 (239)	09:03	39.51, 77.22	32	3.9	240, 78, 0	−6.05 ± 0.54	−5.16 ± 0.00	−5.90 ± 0.00
C12	1999 Mar 04 (063)	05:38	27.91, 57.49	26	10	250, 16, 68	−5.37 ± 0.47	−5.11 ± 0.76	−5.32 ± 0.47
C13	1999 Mar 28 (087)	19:05	30.38, 79.21	30	7.8	280, 7, 75	−4.53 ± 0.29	−3.88 ± 1.00	−4.23 ± 0.73
C14	1999 Jun 15 (166)	20:42	18.44, −97.38	61	31	309, 40, −83	−4.99 ± 0.37	−4.70 ± 0.40	−5.03 ± 0.35
C15	1999 Aug 17 (229)	00:01	40.75, 29.86	17	288	182, 74, 3	−5.70 ± 0.28	−5.33 ± 0.52	−5.53 ± 0.41
C16	1999 Nov 08 (312)	16:45	36.48, 70.81	237	6.4	203, 27, 97	−5.13 ± 0.34	−4.72 ± 0.76	−5.08 ± 0.55
C17	1999 Nov 12 (316)	16:57	40.93, 31.25	18	67	268, 54, −167	−5.14 ± 0.42	−4.21 ± 0.60	−4.53 ± 0.49
C18	2000 Jun 07 (159)	21:47	26.70, 97.15	37	3.7	290, 38, 41	−4.34 ± 0.31	−3.95 ± 0.49	−4.36 ± 0.34
C19	2000 Jul 17 (199)	22:53	36.24, 70.82	146	3.4	310, 26, 153	−5.02 ± 0.37	−3.94 ± 0.85	−4.30 ± 0.73
C20	2000 Oct 02 (276)	02:25	−7.79, 30.60	40	5.7	172, 32, −85	−4.76 ± 0.27	−4.40 ± 0.79	−4.80 ± 0.64
C21	2000 Nov 25 (330)	18:09	40.24, 49.95	15	18	93, 2, −145	−5.79 ± 0.42	−5.14 ± 0.76	−5.41 ± 0.58
C22	2000 Dec 06 (341)	17:11	39.60, 54.87	33	39	319, 33, 136	−4.73 ± 0.34	−3.87 ± 0.71	−4.21 ± 0.54
C23	2001 Jan 26 (026)	03:16	23.42, 70.23	16	340	298, 39, 136	−4.67 ± 0.26	−4.25 ± 0.39	−4.67 ± 0.21
C24	2001 Feb 28 (059)	18:54	47.14, −122.53	47	18	176, 17, −96	−4.93 ± 0.37	−4.48 ± 0.43	−4.73 ± 0.34
C25	2001 Nov 14 (318)	09:26	35.95, 90.54	10	590	94, 61, −12	−6.31 ± 0.41	−5.66 ± 0.51	−6.23 ± 0.58
C26	2002 Feb 03 (034)	07:11	38.62, 31.21	15	6.0	269, 37, −71	−5.54 ± 0.49	−4.92 ± 0.51	−5.33 ± 0.40
C27	2002 Mar 03 (062)	12:08	36.57, 70.42	229	127	282, 22, 85	−4.46 ± 0.33	−4.04 ± 0.69	−4.35 ± 0.55
C28	2002 Jun 22 (173)	02:58	35.82, 48.97	15	7.0	295, 29, 99	−4.72 ± 0.22	−3.88 ± 0.83	−4.39 ± 0.55
C29	2002 Oct 23 (296)	11:27	63.58, −148.13	16	11	262, 89, 179	−5.13 ± 0.39	−4.41 ± 0.94	−4.76 ± 0.75
C30	2002 Nov 03 (307)	22:12	63.52, −147.44	4	750	291, 71, 171	−5.46 ± 0.25	−5.09 ± 0.52	−5.38 ± 0.37
C31	2002 Nov 20 (324)	21:32	35.52, 74.66	15	3.5	204, 30, −117	−5.13 ± 0.31	−4.62 ± 0.83	−5.00 ± 0.70
C32	2003 Feb 24 (055)	02:03	39.37, 77.24	24	3.7	239, 33, 62	−5.50 ± 0.46	−5.17 ± 0.70	−5.55 ± 0.43
C33	2003 Apr 17 (107)	00:48	37.53, 96.45	16	4.1	294, 29, 88	−4.94 ± 0.28	−4.53 ± 0.54	−4.87 ± 0.32
C34	2003 May 01 (121)	00:27	39.04, 40.53	15	3.9	333, 67, −171	−5.28 ± 0.38	−4.69 ± 0.80	−5.11 ± 0.51
C35	2003 Sep 21 (264)	18:16	19.86, 95.72	16	8.6	8, 71, 172	−5.12 ± 0.23	−4.70 ± 0.70	−5.00 ± 0.43
C36	2003 Sep 27 (270)	11:33	50.02, 87.86	15	94	228, 70, 20	−5.27 ± 0.27	−4.20 ± 0.46	−4.70 ± 0.33
C37	2003 Dec 22 (356)	19:16	35.75, −121.15	15	8.5	296, 32, 88	−4.90 ± 0.37	−4.61 ± 0.53	−4.91 ± 0.33
C38	2003 Dec 26 (360)	01:56	29.10, 58.24	15	9.3	172, 59, 167	−5.26 ± 0.44	−4.76 ± 0.62	−5.05 ± 0.41
C39	2004 Apr 05 (096)	21:24	36.52, 70.84	184	6.3	290, 28, 139	−4.64 ± 0.45	−4.11 ± 0.92	−4.45 ± 0.77
C40	2004 May 28 (149)	12:38	36.55, 51.58	22	3.7	119, 24, 72	−4.97 ± 0.34	−3.94 ± 0.88	−4.45 ± 0.60
C41	2005 Apr 07 (097)	20:04	30.24, 83.77	12	3.4	170, 43, −91	−5.14 ± 0.59	−4.73 ± 0.58	−5.04 ± 0.51
C42	2005 Oct 08 (281)	03:50	34.54, 73.59	26	2.9	334, 40, 123	−4.87 ± 0.36	−4.36 ± 0.61	−4.88 ± 0.36
C43	2005 Dec 05 (339)	12:20	−6.23, 29.60	18	18	149, 50, −122	−5.13 ± 0.30	−4.70 ± 0.33	−5.39 ± 0.16
C44	2005 Dec 12 (346)	21:47	36.45, 71.06	210	8.2	279, 40, 106	−4.67 ± 0.33	−3.13 ± 1.58	−3.74 ± 1.18
C45	2006 Feb 22 (053)	22:19	−21.32, 33.58	11	42	325, 27, −114	−4.70 ± 0.25	−3.91 ± 0.54	−4.47 ± 0.27
C46	2007 May 16 (136)	08:56	20.52, 100.89	13	3.4	324, 81, 179	−5.68 ± 0.32	−5.28 ± 0.63	−5.44 ± 0.53
C47	2008 Jan 09 (009)	08:26	32.30, 85.32	13	5.0	206, 46, −75	−4.83 ± 0.68	−4.30 ± 0.62	−4.72 ± 0.59
C48	2008 Mar 20 (080)	22:33	35.43, 81.37	12	54	358, 41, −110	−5.12 ± 0.27	−4.11 ± 0.75	−4.71 ± 0.41
C49	2008 May 12 (133)	06:28	31.44, 104.10	13	9.0	231, 35, 138	−5.08 ± 0.37	−4.55 ± 0.41	−4.87 ± 0.35
C50	2008 Aug 25 (238)	13:22	30.61, 83.51	17	14	30, 48, −48	−5.16 ± 0.36	−4.78 ± 0.50	−5.15 ± 0.34
C51	2008 Aug 27 (240)	01:35	51.76, 104.02	24	3.4	220, 49, −143	−5.66 ± 0.42	−5.49 ± 0.54	−5.69 ± 0.45
C52	2008 Oct 05 (279)	15:53	39.50, 73.64	12	14	246, 38, 78	−5.04 ± 0.36	−4.50 ± 0.64	−4.86 ± 0.44
C53	2008 Oct 06 (280)	08:30	29.66, 90.50	12	3.7	44, 48, −55	−5.19 ± 0.41	−4.93 ± 0.76	−5.28 ± 0.68
C54	2008 Oct 28 (302)	23:10	30.40, 67.48	17	5.1	304, 73, 171	−4.81 ± 0.38	−4.44 ± 0.47	−4.70 ± 0.36
C55	2008 Oct 29 (303)	11:32	30.29, 67.57	12	5.4	324, 68, −178	−5.24 ± 0.25	−4.79 ± 0.53	−5.03 ± 0.38
C56	2008 Nov 10 (315)	01:22	37.51, 95.75	27	4.1	252, 28, 57	−4.80 ± 0.30	−4.40 ± 0.60	−4.75 ± 0.45
C57	2009 Jan 03 (003)	20:23	36.44, 70.36	206	9.2	264, 28, 77	−4.07 ± 0.42	−3.91 ± 0.45	−4.20 ± 0.32
C58	2009 Aug 28 (241)	01:52	37.64, 95.76	12	3.0	295, 31, 102	−4.93 ± 0.69	−4.51 ± 0.39	−4.92 ± 0.26
C59	2010 Jan 12 (012)	21:53	18.61, −72.62	12	44	152, 69, 159	−4.65 ± 0.30	−4.21 ± 0.20	−4.32 ± 0.17
C60	2010 Mar 11 (070)	14:39	−34.54, −72.11	13	21	324, 35, −90	−4.15 ± 0.62	−4.67 ± 0.37	−4.87 ± 0.34
C61	2010 Apr 13 (103)	23:49	33.05, 96.79	16	25	210, 67, 178	−5.27 ± 0.33	−4.68 ± 0.60	−5.09 ± 0.42
C62	2010 Dec 20 (354)	18:42	28.10, 59.11	15	8.3	36, 87, 180	−5.42 ± 0.49	−4.65 ± 0.79	−5.06 ± 0.56
C63	2011 Jan 18 (018)	20:23	28.61, 63.90	52	88	77, 31, −60	−4.76 ± 0.48	−4.12 ± 0.44	−4.49 ± 0.44
C64	2011 Feb 04 (035)	13:53	24.46, 94.68	104	3.1	256, 52, 36	−4.87 ± 0.42	−4.79 ± 0.72	−5.12 ± 0.51
C65	2011 Mar 24 (083)	13:55	20.62, 100.02	13	23	339, 79, 175	−5.55 ± 0.26	−4.80 ± 0.74	−5.12 ± 0.54
C66	2011 Sep 18 (261)	12:40	27.44, 88.35	46	28	216, 72, −12	−5.08 ± 0.44	−4.48 ± 0.55	−4.75 ± 0.41
C67	2011 Oct 23 (296)	10:41	38.64, 43.40	12	63	246, 38, 60	−4.53 ± 0.23	−3.88 ± 0.73	−4.23 ± 0.46
C68	2011 Dec 27 (361)	15:22	51.84, 96.01	16	13	345, 67, 177	−5.29 ± 0.49	−4.58 ± 0.81	−4.95 ± 0.57

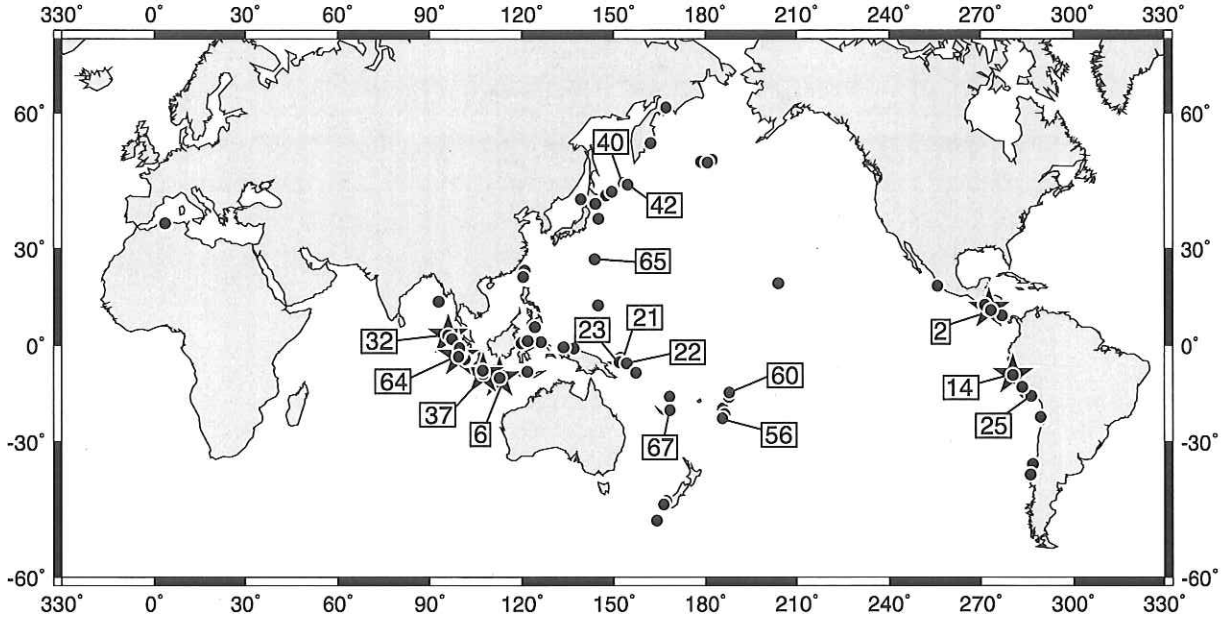

Figure 2. Location map showing earthquakes in comparison (oceanic) data set used to develop regional Θ correction (see Table 1 for earthquake details and Θ results). Tsunami earthquakes plotted as stars; event numbering from Table 1. Non-tsunami earthquakes discussed in Section 3.2 are numbered following Table 1.

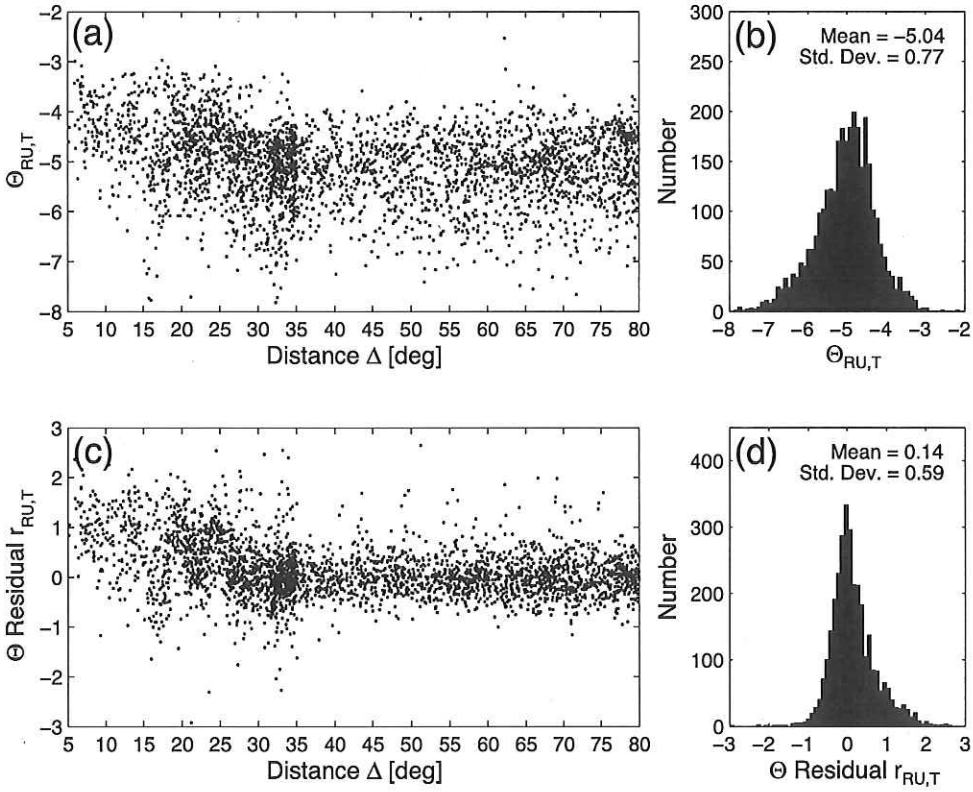

Figure 3. Comparison data set summary ($5° < \Delta < 80°$). (a) Uncorrected regional and teleseismic event-station Θ ($\Theta_{RU,T}$) by epicentral distance Δ with (b) histogram and statistics. (c) Uncorrected regional and teleseismic event-station Θ residuals ($r_{RU,T}$) by epicentral distance Δ with (d) histogram and statistics.

teleseismic residuals as $r_{RU} = \Theta_{RU} - \overline{\Theta_T}$ and $r_T = \Theta_T - \overline{\Theta_T}$, respectively. These data are shown in Fig. 3(c). Fig. 3(d) presents these residuals as a histogram characterized by a mean residual $\bar{r} = 0.14$ and standard deviation $\sigma_r = 0.59$.

Figs 4 and 5 examine separately the teleseismic and regional trends in Θ values and residuals, and confirm both the robustness of Θ_T and the unreliability of Θ_{RU} at epicentral distances less than about 27°. Fig. 4(a) presents the 1665 teleseismic event-station Θ_T values. A mean $\overline{\Theta_T} = -5.18$ and standard deviation $\sigma_\Theta = 0.73$ characterizes this distribution, as shown in the Fig. 4(b) histogram. Teleseismic residuals, plotted in Fig. 4(c) and shown as a histogram in Fig. 4(d), are grouped symmetrically about zero (as by definition

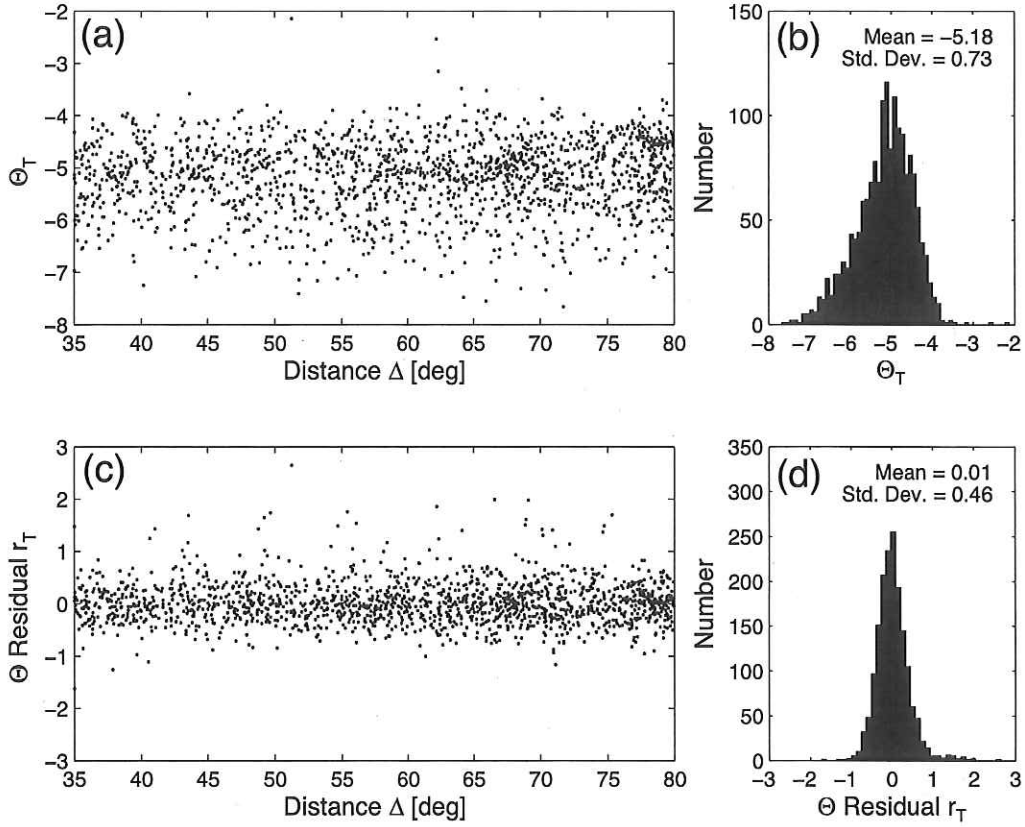

Figure 4. Teleseismic ($35° < \Delta < 80°$) portion of comparison data set. (a) Event-station Θ (Θ_T) by epicentral distance Δ with (b) histogram and statistics. (c) Event-station Θ residuals (r_T) by epicentral distance Δ with (d) histogram and statistics.

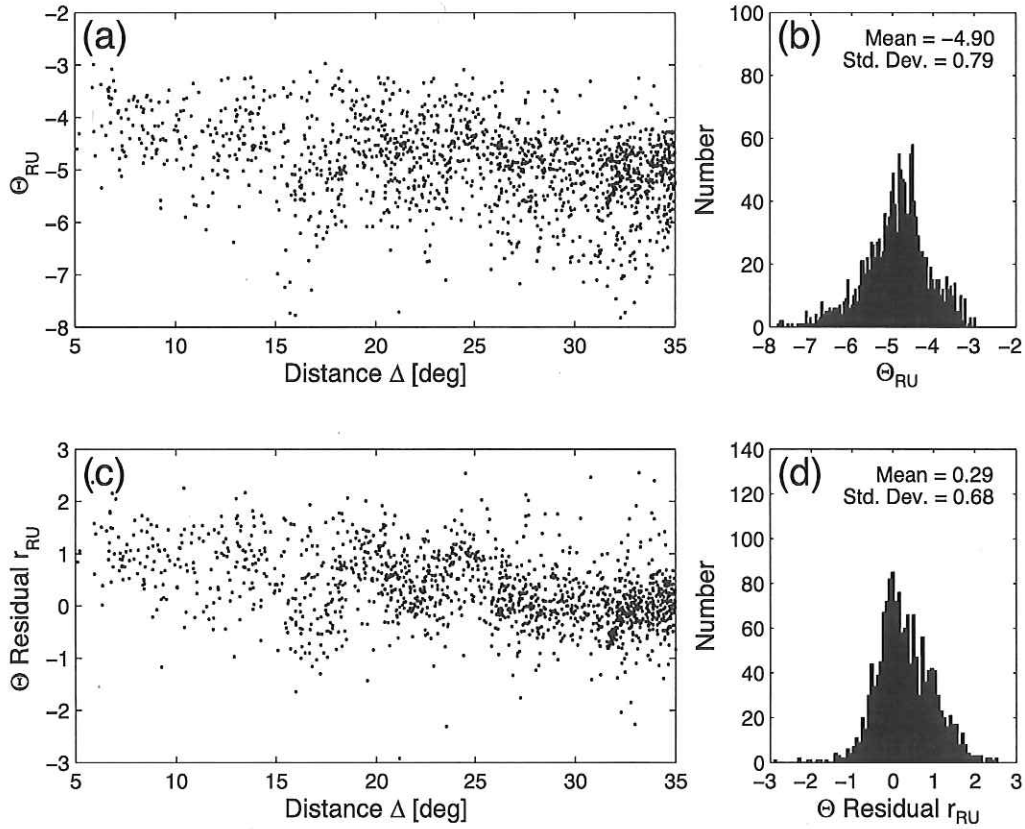

Figure 5. Uncorrected regional ($5° < \Delta < 35°$) portion of comparison data set. (a) Event-station Θ (Θ_{RU}) by epicentral distance Δ with (b) histogram and statistics. (c) Event-station Θ residuals (r_{RU}) by epicentral distance Δ with (d) histogram and statistics.

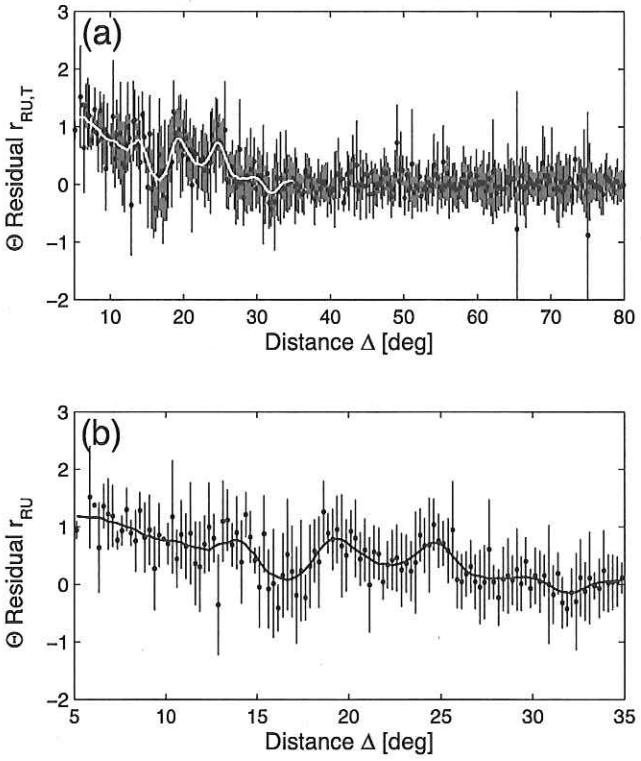

Figure 6. Binned comparison station-event Θ residuals used to develop correction curve. (a) 0.25° bin means with ±1 standard deviations for uncorrected regional ($5° < \Delta < 35°$) and teleseismic ($35° < \Delta < 80°$) portions of the station-event Θ ($\Theta_{RU,T}$) data set. (b) Regional portion of uncorrected station-event Θ (Θ_{RU}) data set. The regional correction curve, shown in Fig. 7(b) (see Table 2), is developed by smoothing bin means and resampling at 0.5° intervals. The negative of the correction curve is shown in white in (a) and black in (b).

they should be). The r_T distribution is described by a mean residual $\overline{r_T} = 0.01$ and standard deviation $\sigma_r = 0.46$.

The distribution of the 1520 uncorrected regional event-station Θ_{RU} values, plotted in Fig. 5(a), is characterized by a mean $\overline{\Theta} = -4.90$, about ~0.3 logarithmic unit more energetic than $\overline{\Theta_T}$, and a standard deviation $\sigma_\Theta = 0.79$ (Fig. 5b). These statistical measures clearly do not fully characterize the skewed distribution, however. As epicentral distances decrease below about 27°, Θ_{RU} values trend increasingly energetic (Fig. 5a). For example, between about 27° and 35°, mean Θ_{RU} compares favourably with the mean teleseismic value ($\Theta \sim -5.2$), while between about 5° and 15°, mean Θ_{RU} is more energetic by about 3/4 logarithmic unit. A similar trend can be seen in Fig. 5(c), which shows uncorrected regional r_{RU} residuals. Local minima and maxima in r_R are particularly notable near caustic distances.

2.3 Comparison data set limitations

As discussed, our focus is on the generalized *P* wave. Regional 70-s windows may contain energy from other arrivals that can contribute to caustic amplitude and distance variations. However, potential bias arising from them is mitigated by averaging within our comparison data set. Bias arising from shallow crustal heterogeneities at regional distances can be minimized but not removed, simply because the vast majority of seismic stations are located on continents. Using only earthquakes taking place in structurally more homogeneous oceanic environments and for which depths *h* range only between 10 and 78 km ($\overline{h} = 28 \pm 14$ km) further minimizes caustic distance variations. At distances less than about 15°, r_R deviations are due to the growing influence with decreasing distance of shallow structure and lateral crustal variations (Burdick 1981). The greatest effects of these variations are avoided by imposing a minimum source–receiver distance of 5° on waveforms used in this study.

We explore possible biasing of regional Θ using a separate data set comprised of only waveforms from continental earthquakes in Section 3.4.

2.4 The empirical regional correction RC(Δ)

We developed a distance-dependent regional correction RC(Δ) to Θ by placing all residuals r_{RU} and r_T in 0.25° bins and smoothing bin means (Figs 6a and b). Resampling this distribution at 0.5° intervals and reversing the polarity of the resulting curve generates the regional correction (Table 2), shown for reference with ray parameter *p* for surface-focus *P* and P_n rays at regional distances in Fig. 7. The correction does not extend to distances greater than 35°, as smoothed bin means approach zero there and their variability

Table 2. Regional Θ correction values as a function of epicentral distance Δ (see Fig. 7).

Δ (°)	Correction	Δ (°)	Correction	Δ (°)	Correction	Δ (°)	Correction
5.0	−1.19	12.5	−0.68	20.0	−0.64	27.5	−0.10
5.5	−1.16	13.0	−0.72	20.5	−0.53	28.0	−0.11
6.0	−1.16	13.5	−0.77	21.0	−0.42	28.5	−0.11
6.5	−1.11	14.0	−0.72	21.5	−0.36	29.0	−0.12
7.0	−1.07	14.5	−0.56	22.0	−0.34	29.5	−0.12
7.5	−1.02	15.0	−0.35	22.5	−0.36	30.0	−0.09
8.0	−0.97	15.5	−0.18	23.0	−0.44	30.5	−0.01
8.5	−0.88	16.0	−0.11	23.5	−0.56	31.0	0.08
9.0	−0.82	16.5	−0.09	24.0	−0.68	31.5	0.13
9.5	−0.78	17.0	−0.17	24.5	−0.72	32.0	0.14
10.0	−0.76	17.5	−0.31	25.0	−0.63	32.5	0.08
10.5	−0.74	18.0	−0.53	25.5	−0.45	33.0	0.04
11.0	−0.67	18.5	−0.72	26.0	−0.28	33.5	0.02
11.5	−0.64	19.0	−0.80	26.5	−0.16	34.0	0.01
12.0	−0.60	19.5	−0.76	27.0	−0.13	34.5	0

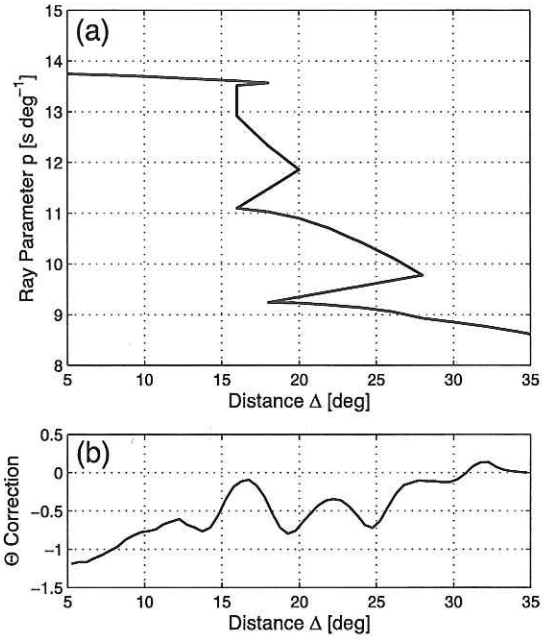

Figure 7. (a) Ray parameter p as a function of distance for surface-focus P and P_n rays bottoming in the upper mantle after ISAPEI1991 model (Kennett 1991). (b) Θ correction as a function of epicentral distance Δ (see Table 2).

becomes comparable (within ±0.1 logarithmic unit) to that seen at greater distances (Fig. 6a).

Our preferred method of developing a regional correction would have been to fit a continuous function to the regional residual r_{RU} data set. However, significant irregularity due to the caustics made it impossible to acceptably represent the residual data set with a simple polynomial.

3 RESULTS

3.1 Application to data set of 67 earthquakes

Here we apply the correction RC(Δ) developed in Section 2.4 to the Θ_{RU} data set to obtain a corrected value $\Theta_{RC} = \Theta_{RU} + RC(\Delta)$. We further define residuals r_{RC} as

$$r_{RC} = \Theta_{RC} - \overline{\Theta_T} = r_{RU} + RC(\Delta). \quad (2)$$

3.1.1 Station-event Θ and r data sets

Mean values referred to in this section are calculated for regional and teleseismic data sets as a whole. Event-averaged Θ is discussed in Section 3.1.2.

The post-correction Θ_{RC} event-station data set is shown in Fig. 8(a). Figs 4 and 8 demonstrate that statistical differences between the corrected regional and teleseismic data sets ($\overline{\Theta_T} = -5.18$

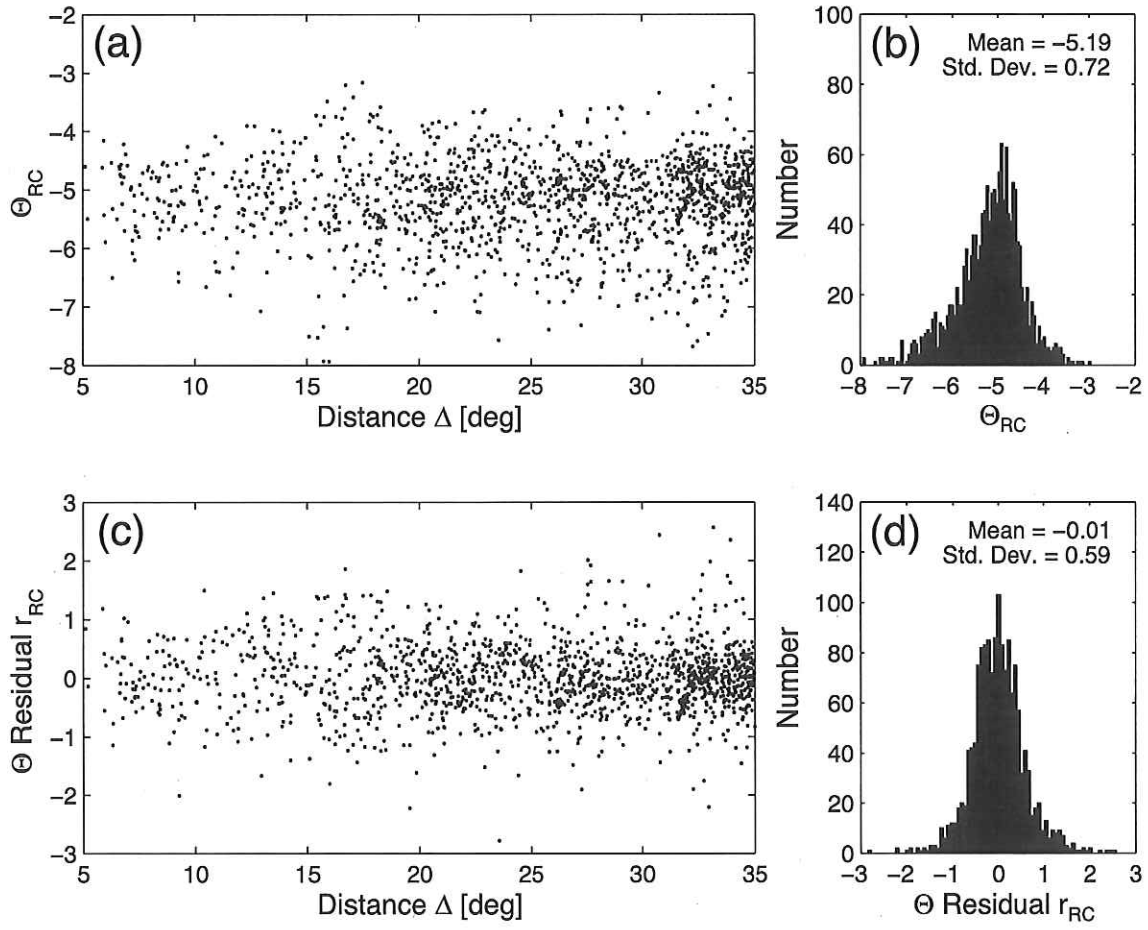

Figure 8. Corrected regional ($5° < \Delta < 35°$) portion of comparison data set. (a) Event-station Θ (Θ_{RC}) by epicentral distance Δ with (b) histogram and statistics. (c) Event-station Θ residuals (r_{RC}) by epicentral distance Δ with (d) histogram and statistics.

Table 3. Statistical summary including mean event-station Θ ($\bar{\Theta}$), mean event-station Θ residual ($\bar{r}$) and number (N) of event-station Θ values for comparison (oceanic) data set used to determine empirical regional Θ correction, and separate validation and continental data sets. Uncertainties are ±1 standard deviation.

Data set	$\bar{\Theta}$	$\bar{r}$	N
Comparison (oceanic)			
Teleseismic	−5.18 ± 0.73	0.01 ± 0.46	1665
Regional (uncorrected)	−4.90 ± 0.79	0.29 ± 0.68	1520
Regional (corrected)	−5.19 ± 0.72	−0.01 ± 0.59	1520
All (with uncorrected regional)	−5.04 ± 0.77	0.14 ± 0.59	3185
All (with corrected regional)	−5.18 ± 0.72	0.00 ± 0.53	3185
Validation			
Teleseismic	−5.00 ± 0.48	0.00 ± 0.37	566
Regional (uncorrected)	−4.61 ± 0.67	0.38 ± 0.66	805
Regional (corrected)	−4.85 ± 0.59	0.14 ± 0.55	805
All (with uncorrected regional)	−4.77 ± 0.63	0.22 ± 0.59	1371
All (with corrected regional)	−4.91 ± 0.55	0.08 ± 0.49	1371
Continental			
Teleseismic	−5.10 ± 0.56	0.00 ± 0.38	1971
Thrust/normal	−4.93 ± 0.51	−0.00 ± 0.39	1207
Hybrid	−5.47 ± 0.66	−0.00 ± 0.40	185
Strike-slip	−5.35 ± 0.47	0.00 ± 0.35	579
Regional (corrected)	−4.90 ± 0.66	0.26 ± 0.53	1380
Thrust/normal	−4.75 ± 0.62	0.17 ± 0.54	613
Hybrid	−5.22 ± 0.86	0.28 ± 0.58	218
Strike-slip	−4.95 ± 0.57	0.35 ± 0.49	549
All (with corrected regional)	−5.02 ± 0.61	0.11 ± 0.47	3351

and $\sigma_{T\Theta} = 0.73$; $\overline{r_T} = 0.01$ and $\sigma_{Tr} = 0.46$) are significantly less than those between the uncorrected regional and teleseismic data sets (see Table 3 for a summary). The post-correction Θ_{RC} data set is characterized by a mean $\overline{\Theta_{RC}} = -5.19$ and standard deviation $\sigma_{RC\Theta} = 0.72$, as shown by the histogram in Fig. 8(b). The residual r_{RC} distribution is plotted in Fig. 8(c); a mean $\overline{r_{RC}} = -0.01$ and standard deviation $\sigma_{RCr} = 0.59$ (Fig. 8d) characterize the distribution. Although standard deviations for Θ_{RC} (0.72) and Θ_T (0.73) are comparable, the r_{RC} standard deviation (0.59) remains about 30 per cent above that of the r_T data set (0.46).

The entire 3,185-point Θ and r data sets, with corrected regional values, are shown in Figs 9(a) and (c). A comparison of the histograms for these distributions (Figs 9b and d) with those for the teleseismic distributions (Figs 4b and d, respectively) demonstrates that corrected regional and teleseismic Θ and r data sets are statistically similar to teleseismic Θ and r distributions (Table 3).

3.1.2 *Event-averaged Θ ($\overline{\Theta_{R,T}}$)*

Here we discuss the effect of correction on event-averaged Θ values for the 67 comparison (oceanic) earthquakes (teleseismic, uncorrected regional, and corrected regional event-averaged Θ results for these events are summarized in Table 1). Fig. 10 compares teleseismic event-averaged theta ($\overline{\Theta_T}$) with uncorrected regional event-averaged theta ($\overline{\Theta_{RU}}$) for individual earthquakes and, like the uncorrected regional event-station Θ values plotted in Fig. 5, confirms that $\overline{\Theta_{RU}}$ values are systematically overestimated with respect to $\overline{\Theta_T}$ values. Positive deviation from the ideal $\overline{\Theta_{RU}} = \overline{\Theta_T}$ relationship can reach about 1 logarithmic unit, while $\overline{\Theta_{RU}}$ for no earthquake is overly deficient (in a statistically significant sense) with respect to $\overline{\Theta_T}$. A regression with a correlation coefficient of 0.91 though the 67 points recovers a best least-squares linear fit of $\overline{\Theta_{RU}} = 0.94\overline{\Theta_T} - 0.08$. At Θ values of greatest interest to tsunami earthquake discrimination ($\Theta < -5.8$), this fit deviates from the ideal teleseismic–regional Θ relationship by about 0.3 logarithmic unit.

By contrast, a regression with a correlation coefficient of 0.91 recovers an improved best linear fit of $\overline{\Theta_{RC}} = 0.91\overline{\Theta_T} - 0.54$ after RC application (Fig. 11). This fit is indistinguishable from the ideal $\overline{\Theta_{RC}} = \overline{\Theta_T}$ relationship within the range of observed Θ values.

3.2 Earthquakes with anomalous Θ

In this section, we verify that corrected Θ detects anomalous events not following scaling laws in general, and tsunami earthquakes in particular. We refer to an earthquake as slow if $\Theta < -6.0$ logarithmic units; intermediate slow if $-6.0 < \Theta < -5.8$; mainstream if $-5.8 < \Theta < -4.5$ and fast if $\Theta > -4.5$.

3.2.1 *Tsunami earthquakes*

Six earthquakes within the past two decades are recognized as tsunami earthquakes and are associated with $\overline{\Theta_T}$ values deficient as much as two logarithmic units (Newman & Okal 1998; Choy & Boatwright 2007; Stein & Okal 2007; Fritz *et al.* 2007; Newman *et al.* 2011, see earthquakes highlighted in Table 1, denoted with stars in Fig. 2, and accompanied by open circles and bolded event numbers in Figs 10 and 11) . Based on $\overline{\Theta_{RU}}$ values alone, the 1992 September 2 Nicaragua (Event 2), 1994 June 2 Java (Event 6), 2004 December 26 Sumatra (Event 32) and 2006 July 17 Java (Event 37) earthquakes are classified as slow, with $\overline{\Theta_{RU}}$ values of -6.44 ± 0.59, -6.70 ± 0.39, -6.82 ± 0.41 and -6.04 ± 0.82, respectively. However, the remaining two tsunami earthquakes, in Peru, 1996 February 21 (Event 14); and Mentawai, 2010 October 25 (Event 64), feature mainstream $\overline{\Theta_{RU}}$ values of -5.67 ± 0.30 and -5.46 ± 0.59, respectively.

Since the application of RC reduces Θ values, no tsunami earthquake classification is lost through the correction of regional $\overline{\Theta}$. $\overline{\Theta_{RC}}$ values of slow earthquakes [Events 2 (-6.70 ± 0.36), 6 (-6.81 ± 0.32), 32 (-6.92 ± 0.40) and 37 (-6.38 ± 0.74)] are slightly more deficient than $\overline{\Theta_T}$ values, and with correction Event 14 becomes classified as intermediate slow (-5.90 ± 0.30). The increased deficiency (-5.78 ± 0.46) of Event 64 borders on intermediate-slow.

Because our focus is on the extension of a formal Θ algorithm to regional distances within the context of tsunami warning, we consistently use a fixed 70-s window of integration (as discussed in Section 2.2). Our teleseismic and corrected regional Θ thus underestimate the energy of the 2004 December 26 Sumatra earthquake (Event 32), which due to its great size and extraordinary source duration can never be fully described by a regular energy estimation algorithm (Stein & Okal 2005, 2007; Tsai *et al.* 2005; Seno & Hirata 2007). Indeed, using a 500-s window, Choy & Boatwright (2007) still obtain a deficient energy value equivalent to $\Theta = -5.9$.

3.2.2 *Other earthquakes with deficient Θ*

Here we briefly discuss three earthquakes having characteristics not consistent with true tsunami earthquakes, but for which $\overline{\Theta_{RC}}$ values are nonetheless deficient. In each case, $\overline{\Theta_{RC}}$ values are consistent with $\overline{\Theta_T}$ values, and correction reduces the difference between regional and teleseismic Θ (each event denoted in Figs 10 and 11 with non-bolded event numbers).

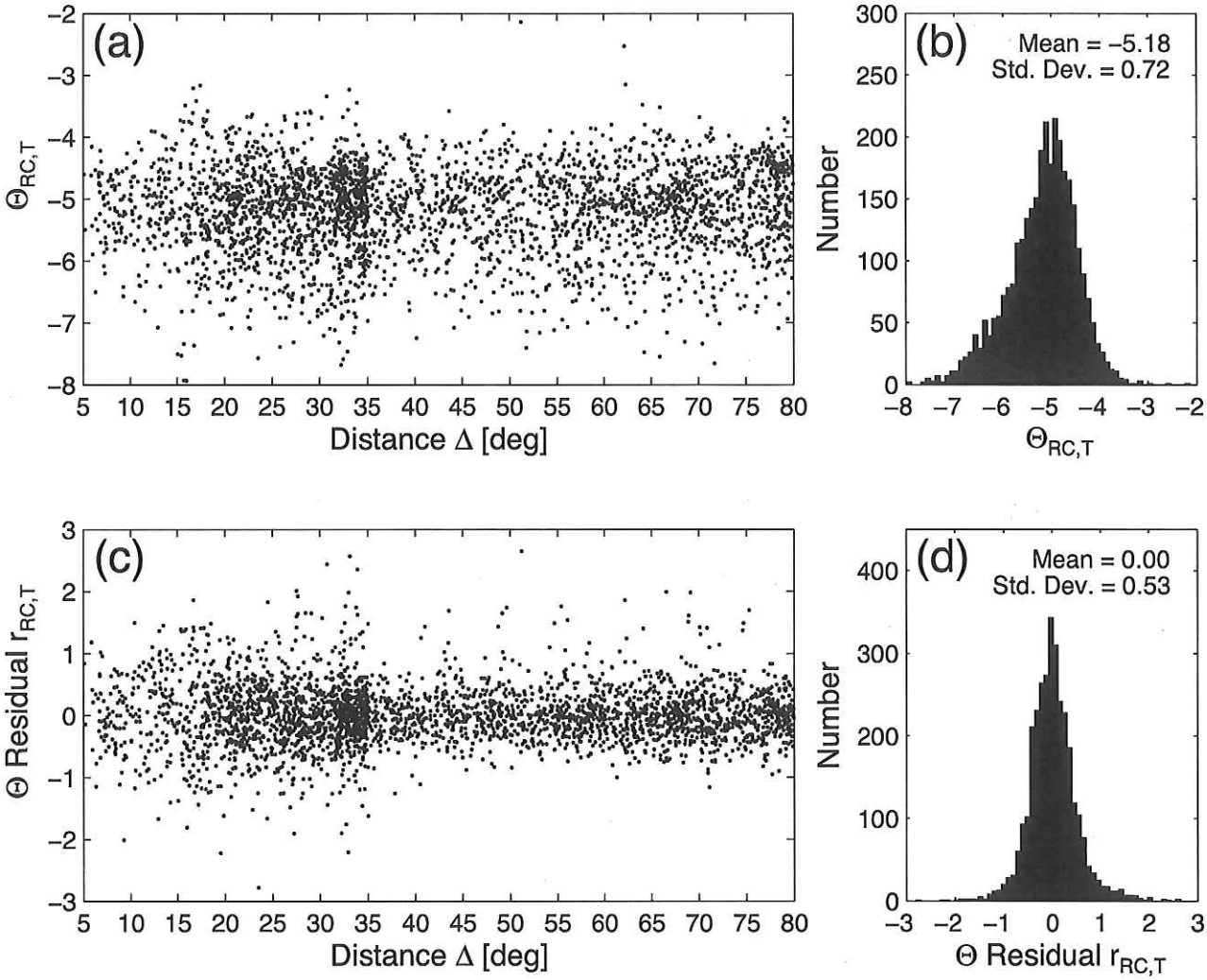

Figure 9. Comparison data set summary ($5° < \Delta < 80°$). (a) Corrected regional and teleseismic event-station Θ ($\Theta_{RC,T}$) by epicentral distance Δ with (b) histogram and statistics. (c) Corrected regional and teleseismic event-station Θ residuals ($r_{RC,T}$) by epicentral distance Δ with (d) histogram and statistics.

New Britain, 2000 November 16–17 (Events 21–23). This thrust-dominated $M_w = 8.0$ (12.4×10^{27} dyn cm) earthquake (Event 21), which ruptured the Weitin Fault between New Britain and New Ireland at the South Bismarck–Pacific Plate boundary (Tregoning *et al.* 2005), was followed during the next 2 d by two large interplate aftershocks triggered by static stress changes induced by the main shock (Geist & Parsons 2005). Our mainstream corrected regional ($\overline{\Theta_{RC}} = -5.57 \pm 0.49$) and teleseismic Θ values ($\overline{\Theta_T} = -5.57 \pm 0.38$) reflect the slightly slow but otherwise unremarkable nature of the main shock.

The first aftershock (Event 22) occurred at the New Britain Trench south of the main shock and to the northeast of the Solomon Sea Plate–Pacific Plate–South Bismarck Plate triple junction. This $M_w = 7.8$ (6.5×10^{27} dyn cm) event was characterized by a simple 35-s moment release in the form of a large pulse followed by a smaller pulse. Our mainstream $\overline{\Theta_{RC}} = -5.71 \pm 0.66$ and $\overline{\Theta_T} = -5.68 \pm 0.46$ values, similar to those of the main shock, are again indicative of a typical event exhibiting a trend towards slowness, in agreement with the best-fit rupture velocity of 2.7 km s^{-1} (Park & Mori 2007).

The second aftershock (Event 23), a $M_w = 7.8$ (5.6×10^{27} dyn cm) interplate event on the New Britain Trench to the west of the first aftershock, however, is characterized by significantly deficient corrected regional ($\overline{\Theta_{RC}} = -6.12 \pm 0.62$) and teleseismic Θ ($\overline{\Theta_T} = -6.11 \pm 0.44$) values, slightly more deficient but consistent with the $\Theta = -5.9$ of Convers & Newman (2011). Such deficiency reflects the relatively slow rupture velocity of only 2.5 km s^{-1} (Park & Mori 2007). This value is comparable, for example, to that of the great Sumatra earthquake of 2004 (Ishii *et al.* 2005; Tolstoy & Bohnenstiehl 2005), but not typical of true tsunami earthquakes, which are characterized by rupture velocities as slow as 1 km s^{-1} (Polet & Kanamori 2000; López & Okal 2006). Further investigation to resolve the case of this event lies outside the scope of this paper.

Both the main shock (Event 21) and first aftershock (Event 22) generated tsunamis (Geist & Parsons 2005), with run-up measurements of 3 m recorded on Bougainville, Buka and Kiriwina (NOAA Geophysical Data Center; http://www.ngdc.noaa.gov/nndc/struts/results?EQ_0=2352&t=101650&s=9&d=92,183&nd=display). Tsunami damage was also observed on the southwest coast of New Ireland (Lander *et al.* 2003). No tsunami was generated by the second aftershock (Event 26).

Peru, 2001 June 23 (Event 25). This $M_w = 8.4$ ($M_0 = 47.0 \times 10^{27}$ dyn cm) underthrusting earthquake on the Nazca–South America Plate boundary generated a tsunami observed for more than

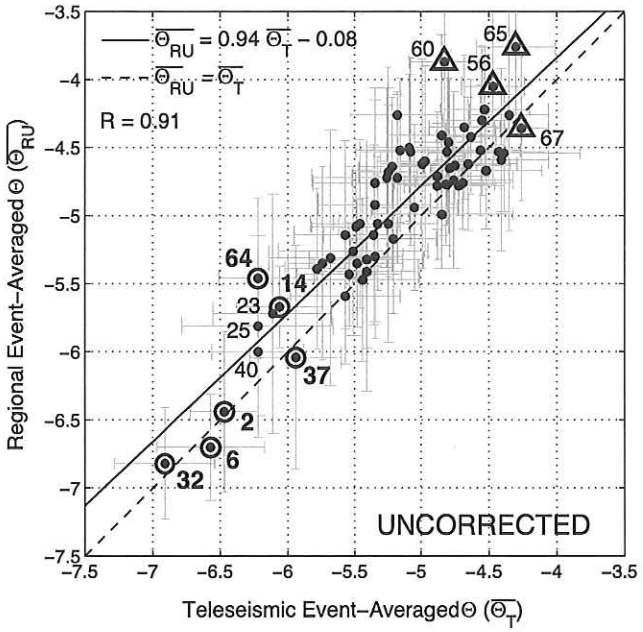

Figure 10. Teleseismic event-averaged theta ($\overline{\Theta_T}$) values (horizontal axis) versus uncorrected regional event-averaged theta ($\overline{\Theta_{RU}}$) values (vertical axis) for comparison data set. Solid line shows best linear fit; dashed line expresses ideal relationship between regional and teleseismic theta (i.e. $\overline{\Theta_{RU}} = \overline{\Theta_T}$). Tsunami earthquakes (highlighted in Table 1 and Fig. 2) are surrounded by open circles and denoted by bolded event number. Other deficient earthquakes discussed in Section 3.2.2 are denoted with non-bolded event number. Fast earthquakes discussed in Section 3.2.3 are surrounded by triangles and denoted with non-bolded event number. Error bars represent ±1 standard deviation (see Table 1) with length of bar-end ticks on one leg proportional to standard deviation of other dimension.

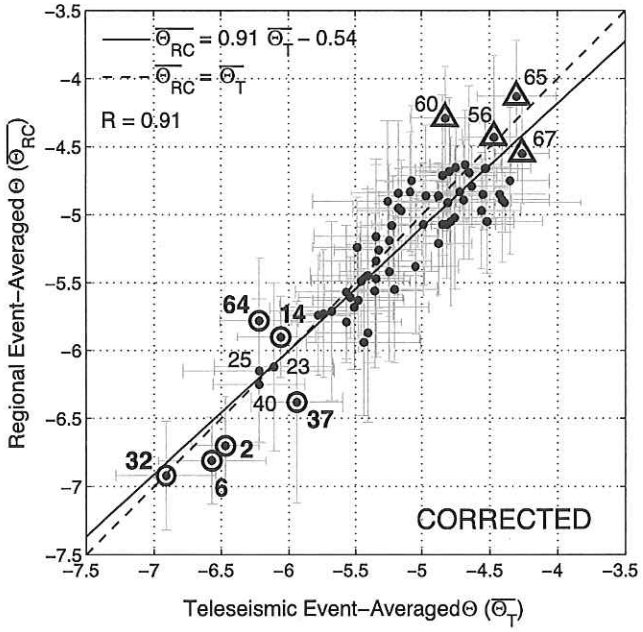

Figure 11. Same as for Fig. 10, but with corrected regional event-averaged theta ($\overline{\Theta_{RC}}$) values (vertical axis).

400 km along the coastline of southern Peru. Maximum tsunami run-up amplitudes approached 7–8 m in some places, and inundations exceeded 1 km in the area of Camaná (Okal *et al.* 2002). Both corrected regional ($\overline{\Theta_{RC}} = -6.15 \pm 0.53$) and teleseismic ($\overline{\Theta_T} = -6.22 \pm 0.56$) Θ values are significantly deficient and characteristic of a tsunami earthquake. However, source studies indicate that moment was released in multiple pulses, with the majority after ~60 s (Giovanni *et al.* 2002; Bilek & Ruff 2002). By using a shifted window appropriate for such a delayed moment release, Weinstein & Okal (2005) obtain a more realistic value of $\overline{\Theta_T} = -5.65$. Using a window delay of 60 s, we obtain here a Θ_{RC} value of −5.4 consistent with their results and moment release studies. Thus this event is more accurately described as delayed rather than slow.

Such characterization is confirmed by this event's ratio of *T*-phase energy flux to seismic moment, intermediate between the $M_w = 7.5$ tsunami earthquake of 1996 February 21 (Event 14) and the regular $M_w = 7.7$ Nazca event of 1996 November 12 (Event 16; Okal *et al.* 2002).

Kuril Islands, 2006 November 15 (Event 40). The great Kuril Islands interplate earthquake of 2006 November 15 ($M_w = 8.3$; $M_0 = 33.7 \times 10^{27}$ dyn cm) ruptured the plate boundary where the Pacific Plate subducts beneath the central Kuril arc. The event generated a tsunami significant in the near field (MacInnes *et al.* 2009) but only modest in the far field (Fujii & Satake 2008). Significant far-field damage was reported only in the harbour at Crescent City, California, USA, due to a series of late waves reaching a maximum peak-to-peak amplitude of ~1.7 m there (Dengler *et al.* 2009).

Both corrected regional ($\overline{\Theta_{RC}} = -6.25 \pm 0.42$) and teleseismic ($\overline{\Theta_T} = -6.22 \pm 0.34$) Θ values are significantly deficient and characteristic of a tsunami earthquake. A slow average rupture velocity of 1.8 km s^{-1}, a slow rise time and a total duration exceeding 120 s supports this assessment (Ammon *et al.* 2008; Lay *et al.* 2009). Using a window delay of ~30 s shifts both Θ_T and Θ_{RC} to less-deficient mainstream values of ~−5.6 consistent with these observations. Thus this earthquake is better described as delayed rather than slow, similar to the 2001 June 23 Peru earthquake (Event 25) discussed earlier.

The November 15 event was followed by a nearby $M_w = 8.1$ shallow outer rise intraplate normal faulting event on 2007 January 13 (Event 42), one of the largest recorded outer rise normal faulting events (Ammon *et al.* 2008). In contrast to the first event of the couplet, the 2007 event is characterized by mainstream Θ values trending towards fast or 'snappy' ($\overline{\Theta_{RC}} = -5.02 \pm 0.53$ and $\overline{\Theta_T} = -4.76 \pm 0.44$). This characterization is consistent with an increased rupture velocity of 3.5 km s^{-1} (Lay *et al.* 2009) and a source enriched in short-period energy that has a sharp rise time and releases moment over only ~40 s (Ammon *et al.* 2008; Lay *et al.* 2009).

3.2.3 *Fast earthquakes*

At the opposite end of the slowness spectrum lie four outer rise intraplate earthquakes (each denoted in Figs 10 and 11 with triangles and non-bolded Table 1 event numbers) taking place near Tonga, on 2009 March 19 (Event 56); Samoa, on 2009 September 29 (Event 60); in the Bonin Islands, on 2010 December 21 (Event 65); and near Vanuatu, on 2011 January 13 (Event 67). Corrected regional Θ_{RC} values (−4.43 ± 0.60, −4.29 ± 0.38, −4.13 ± 0.41 and −4.55 ± 0.37, respectively) for these earthquakes are either fast or borderline so. Such characterization, consistent with expected 'snappiness' due to the intraplate nature of these events, is compatible with energetic

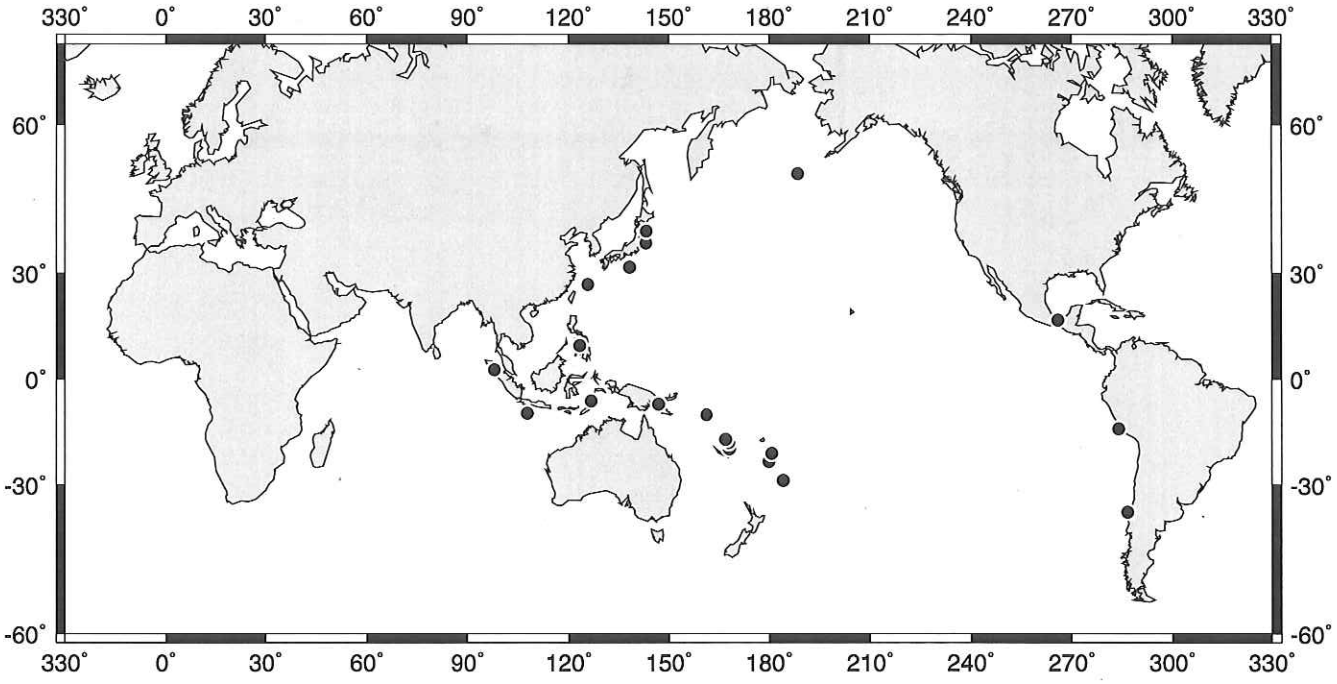

Figure 12. Location map for validation events included in this study (see Table 1 for earthquake details and Θ results).

teleseismic Θ_T values (-4.47 ± 0.23; -4.83 ± 0.26; -4.30 ± 0.29 and -4.26 ± 0.20, respectively).

3.3 Application to independent validation events (V1–V23)

To assess the general validity of our regional Θ correction RC, we correct 23 additional events (shown in Fig. 12 and summarized in Table 1) not included in the data set of 67 earthquakes used in the empirical determination of the regional correction. Although smaller, the validation data set mirrors the larger data set and is thus comprised of only earthquakes taking place in oceanic environments and having focal geometries with null axes plunging shallower than 50° (the median null axis plunge for validation events is 11°). With the exception of the great $M_0 = 530 \times 10^{27}$ dyn cm ($M_w = 9.1$) Tohoku earthquake of 2011 March 11 (Event V3), validation data set seismic moments fall between 1.3×10^{26} dyn cm and 3.0×10^{27} dyn cm ($6.7 < M_w < 7.6$).

As shown in Fig. 13, a regression with a correlation coefficient $R = 0.60$ though the 23 points recovers a best least-squares linear fit of $\overline{\Theta_{RU}} = 0.54\overline{\Theta_T} - 1.94$ between the teleseismic and uncorrected regional validation event-averaged Θ values. Fig. 14 shows that the fit improves to $R = 0.72$ after regional Θ correction application such that $\overline{\Theta_{RC}} = 0.74\overline{\Theta_T} - 1.23$. Teleseismic and corrected regional Θ values for all validation events, including the tsunamigenic great Tohoku earthquake ($\overline{\Theta_{RC}} = -5.50 \pm 0.40$ and $\overline{\Theta_T} = -5.59 \pm 0.45$), are characterized as mainstream.

Station-event mean values are statistically consistent for the corrected regional ($\Theta_{RC} = -4.85 \pm 0.59$) and teleseismic ($\Theta_T = -5.00 \pm 0.48$) data sets. Because no recognized tsunami earthquakes are included in the validation data set, teleseismic and corrected regional Θ means for it are about 0.2–0.3 logarithmic units less deficient than corresponding means for the comparison data set (Table 3).

We conclude that application of the regional Θ correction recovers an accurate and robust measurement of an event's slowness fully consistent with Θ calculated using only waveforms recorded at teleseismic distances.

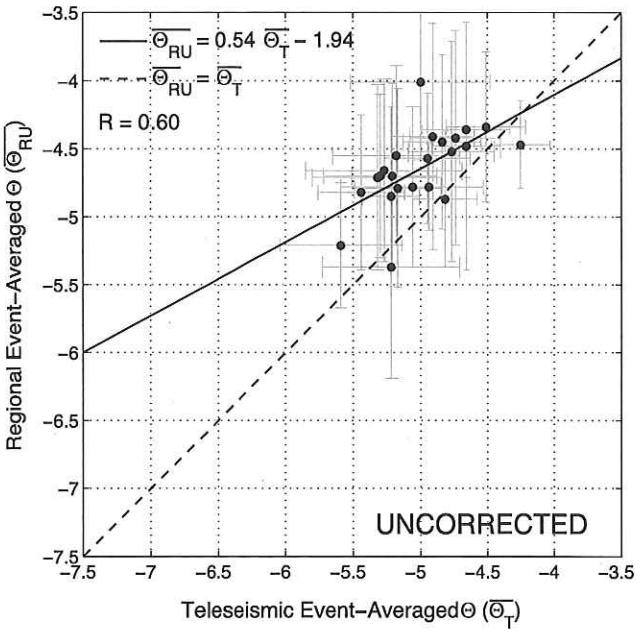

Figure 13. Teleseismic event-averaged theta ($\overline{\Theta_T}$) values (horizontal axis) versus uncorrected regional event-averaged theta ($\overline{\Theta_{RU}}$) values (vertical axis) for validation data set. Solid line shows best linear fit; dashed line expresses ideal relationship between regional and teleseismic theta (i.e. $\overline{\Theta_{RU}} = \overline{\Theta_T}$). Error bars represent ±1 standard deviation (see Table 1) with length of bar-end ticks on one leg proportional to standard deviation of other dimension.

3.4 Continental data set events (C1–C68)

Here we explore whether the use of waveforms from continental earthquakes traversing primarily continental structure indeed biases

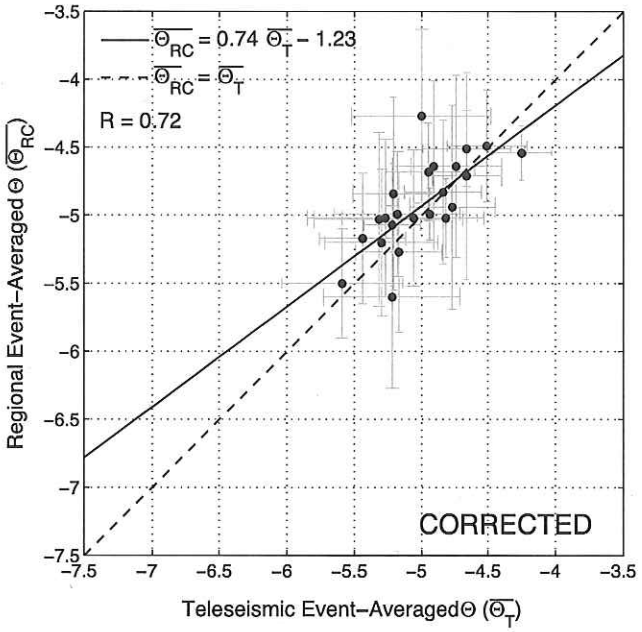

Figure 14. Same as for Fig. 13, but with corrected regional event-averaged theta ($\overline{\Theta_{RC}}$) values (vertical axis).

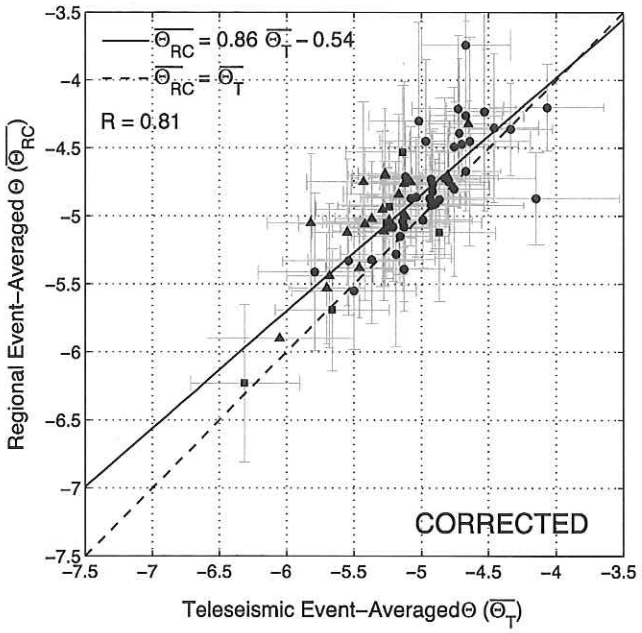

Figure 16. Teleseismic event-averaged theta ($\overline{\Theta_T}$) values (horizontal axis) versus corrected regional event-averaged theta ($\overline{\Theta_{RC}}$) values (vertical axis) for entire continental data set. Solid line shows best linear fit; dashed line expresses ideal relationship between regional and teleseismic theta (i.e. $\overline{\Theta_{RC}} = \overline{\Theta_T}$). Circles represent thrust and normal (null axis plunge $< 30°$), squares hybrid ($31° <$ null axis plunge $< 60°$) and triangles strike-slip ($61° <$ null axis plunge $< 90°$) events. Error bars represent ± 1 standard deviation (see Table 1) with length of bar-end ticks on one leg proportional to standard deviation of other dimension.

regional Θ for broad focal mechanism categories, similar to the work of Convers & Newman (2011), who focus on focal mechanism dependence of Θ for large earthquakes occurring globally.

Our additional data set is comprised of 68 continental earthquakes taking place between 1996 and 2012 (Table 1 and Fig. 15) with varying focal geometries. Null axis plunge divides these events into thrust- or normal-dominated ($0° \leq$ plunge $< 30°$; 41 events with median plunge 11°), hybrid ($30° <$ plunge $< 60°$; 6 events with median plunge 54.5°) and strike-slip ($60° <$ plunge $< 90°$; 21 events with median plunge 69°) subsets. Following the procedure outlined in Section 2.2, we calculate event-averaged Θ using regional and teleseismic waveforms. We then compare $\overline{\Theta_{RC}}$ with $\overline{\Theta_T}$, which is much less sensitive to shallow crustal structure and upper-mantle heterogeneities because of steeper take-off angles. Teleseismic and corrected regional Θ are compared for the entire 68-earthquake continental data set in Fig. 16. Because we remain cognizant of energy

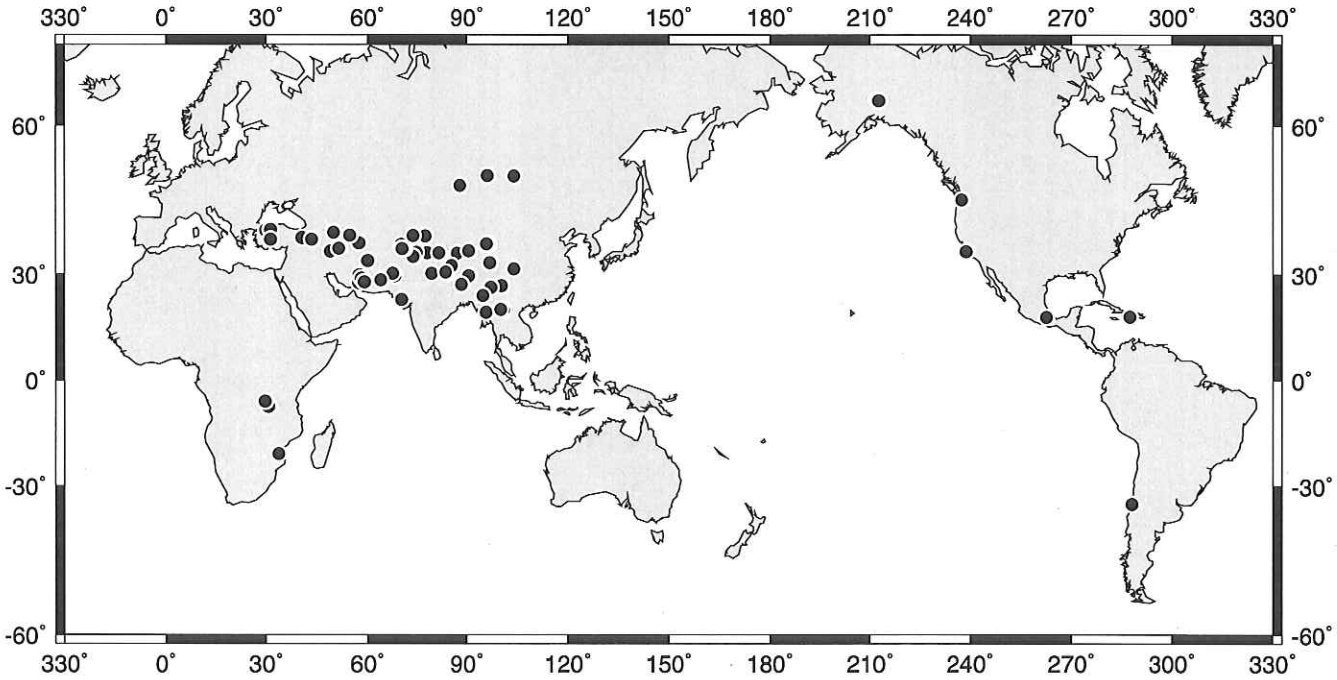

Figure 15. Location map for continental events included in this study (see Table 1 for earthquake details and Θ results).

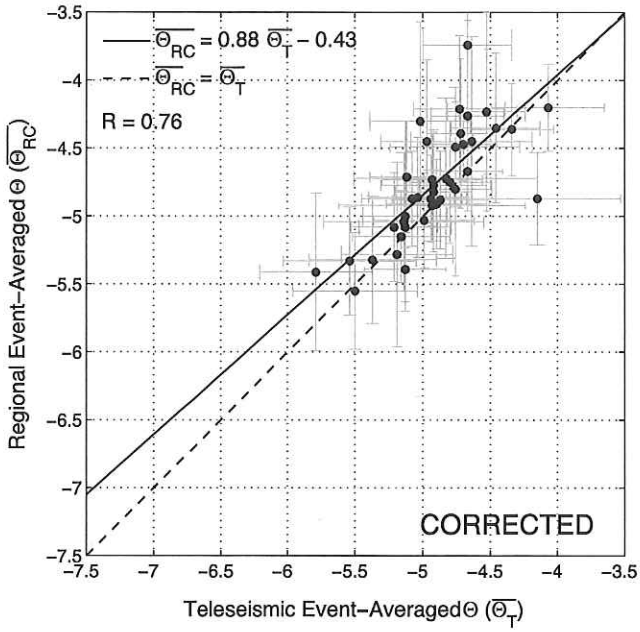

Figure 17. Teleseismic event-averaged theta ($\overline{\Theta_T}$) values (horizontal axis) versus corrected regional event-averaged theta ($\overline{\Theta_{RC}}$) values (vertical axis) for continental data set thrust and normal events (null axis plunge $< 30°$). Solid line shows best linear fit; dashed line expresses ideal relationship between regional and teleseismic theta (i.e. $\overline{\Theta_{RC}} = \overline{\Theta_T}$). Error bars represent ± 1 standard deviation (see Table 1) with length of bar-end ticks on one leg proportional to standard deviation of other dimension.

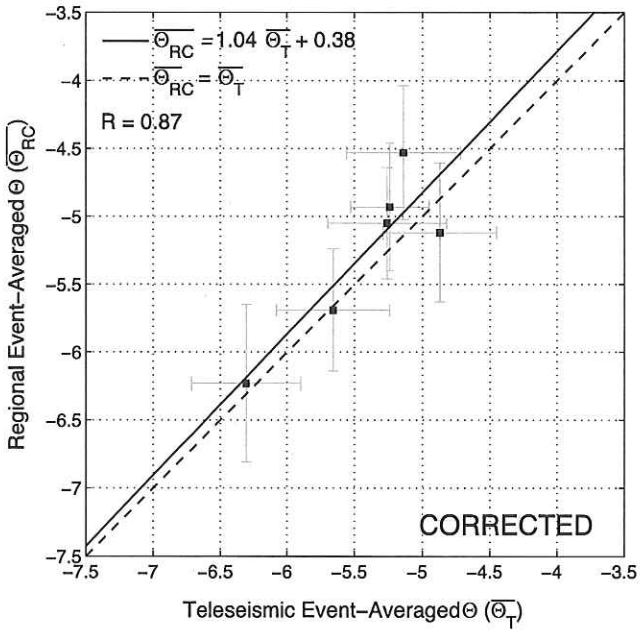

Figure 18. Teleseismic event-averaged theta ($\overline{\Theta_T}$) values (horizontal axis) versus corrected regional event-averaged theta ($\overline{\Theta_{RC}}$) values (vertical axis) for continental data set hybrid events ($31° <$ null axis plunge $< 60°$). Solid line shows best linear fit; dashed line expresses ideal relationship between regional and teleseismic theta (i.e. $\overline{\Theta_{RC}} = \overline{\Theta_T}$). Error bars represent ± 1 standard deviation (see Table 1) with length of bar-end ticks on one leg proportional to standard deviation of other dimension.

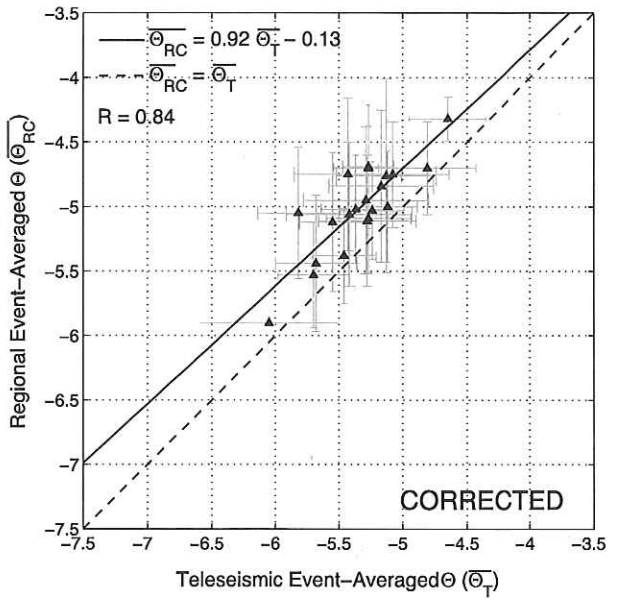

Figure 19. Teleseismic event-averaged theta ($\overline{\Theta_T}$) values (horizontal axis) versus corrected regional event-averaged theta ($\overline{\Theta_{RC}}$) values (vertical axis) for continental data set strike-slip events ($61° <$ null axis plunge $< 90°$). Solid line shows best linear fit; dashed line expresses ideal relationship between regional and teleseismic theta (i.e. $\overline{\Theta_{RC}} = \overline{\Theta_T}$). Error bars represent ± 1 standard deviation (see Table 1) with length of bar-end ticks on one leg proportional to standard deviation of other dimension.

bias related to strike-slip geometries when waveforms are recorded at teleseismic distances as discussed in Section 1.1.1, and problems associated with caustics at regional distances as discussed in Section 2.3, we are able to draw only broad conclusions based on relative differences between continental earthquake subsets.

Fig. 17 compares teleseismic and corrected regional Θ for thrust- and normal-dominated continental events. A regression with a correlation coefficient of 0.76 though the 41 points recovers a best least-squares linear fit of $\overline{\Theta_{RU}} = 0.88\overline{\Theta_T} - 0.43$. Within the range of Θ values represented ($-4 < \Theta < -5.5$), this fit is slightly biased to more energetic values of regional Θ by $\sim$0.2 logarithmic unit compared to the best-linear fit for corrected oceanic $\overline{\Theta_{RC}}$ and $\overline{\Theta_T}$, shown in Fig. 11. Shallow heterogeneities arising from more complex continental crustal structure thus appear to lead to overestimation of Θ when regional waveforms from continental earthquakes with shallow null axes are used, but this bias is small compared with typical Θ uncertainties.

The small number of events precludes any definitive statistical characterization of the hybrid data set (for which teleseismic and corrected regional Θ are compared in Fig. 18).

Fig. 19 shows that teleseismic Θ is underestimated by about 0.3 logarithmic unit with respect to corrected regional Θ. This difference could express bias due to shallow crustal heterogeneities, but we instead prefer to interpret it as an underestimation of teleseismic Θ within the framework of our methodology, which ignores focal mechanism corrections.

4 CONCLUSIONS

Newman & Okal's (1998) algorithm Θ results are robust for waveforms recorded at teleseismic epicentral distances (i.e. for $\Delta > 30°$), but are unreliable for distances less than 30°. This discrepancy is

due primarily to the use at caustic source–receiver distances of a smoothed traveltime curve ($d^2T/d\Delta^2$) in the determination of the geometrical spreading factor necessary to calculate the estimated radiated energy E^E. Local-scale heterogeneity and crustal structure contribute to this discrepancy, especially at shorter epicentral distances.

We show that regional Θ values obtained by the application of a regional correction developed here are comparable to those calculated using waveforms recorded at only teleseismic epicentral distances. Based on deficient Θ values, corrected regional Θ is able to correctly distinguish known tsunami earthquakes, identify all anomalous 'slow' events consistent with their characterization using teleseismic Θ and does not identify any anomalous events with Θ inconsistent with teleseismic values.

ACKNOWLEDGMENTS

We thank the IRIS DMC for data access. Some figures were generated using the Generic Mapping Tools (GMT) software (Wessel & Smith 1991). Helpful comments from two anonymous reviewers significantly improved the manuscript. This work was supported by a National Science Foundation Graduate Research Fellowship to CWE under Grant Number DGE-0824162.

REFERENCES

Ammon, C., Kanamori, H. & Lay, T., 2008. A great earthquake doublet and seismic stress transfer cycle in the Central Kuril islands, *Nature,* **451,** 561–656, doi:10.1038/nature06521.

Bilek, S. & Ruff, L., 2002. Analysis of the 23 June 2001 $M_W = 8.4$ Peru underthrusting earthquake and its aftershocks, *Geophys. Res. Lett.,* **29**(20), doi:10.1029/2002GL015543.

Boatwright, J. & Choy, G., 1986. Teleseismic estimates of the energy radiated by shallow earthquakes, *J. geophys. Res.,* **91**(B2), 2095–2112.

Burdick, L., 1981. A comparison of the upper mantle structure beneath North America and Europe, *J. geophys. Res.,* **86**(B7), 5926–5936.

Burdick, L. & Helmberger, D., 1978. The upper mantle *P* velocity structure of the western United States, *J. geophys. Res.,* **83**(B4), 1699–1712.

Choy, G. & Boatwright, J., 2007. The energy radiated by the 26 December 2004 Sumatra-Andaman earthquake estimated from 10-minute *P*-wave windows, *Bull. seism. Soc. Am.,* **97**(1S), S25–S42, doi:10.1785/0120050626.

Choy, G. & McGarr, A., 2002. Strike-slip earthquakes in the oceanic lithosphere: observations of exceptionally high stress, *Geophys. J. Int.,* **150**(2), 506–523, doi:10.1046/j.1365-246X.2002.01720.x.

Convers, J. & Newman, A., 2011. Global evaluation of large earthquake energy from 1997 through mid-2010, *J. geophys. Res.,* **116,** B08304, doi:10.1029/2010JB007928.

Dengler, L., Uslu, B., Barberopoulou, A., Yim, S. & Kelly, A., 2009. The November 15, 2006 Kuril Islands-generated tsunami in Crescent City, California, *Pure appl. Geophys.,* **166,** 37–53.

Fritz, H. *et al.*, 2007. Extreme runup from the 17 July 2006 Java tsunami, *Geophys. Res. Lett.,* **34,** L12602, doi:10.1029/GL029404.

Fujii, Y. & Satake, K., 2008. Tsunami sources of the November 2006 and January 2007 Great Kuril Earthquakes, *Bull. seism. Soc. Am.,* **98**(3), 1559–1571, doi:10.1785/0120070221.

Gaherty, J., Kato, M. & Jordan, T., 1999. Seismological structure of the upper mantle: a regional comparison of seismic layering, *Phys. Earth planet. Inter.,* **110,** 21–41.

Geist, E. & Parsons, T., 2005. Triggering of tsunamigenic aftershocks from large strike-slip earthquakes: analysis of the November 2000 New Ireland earthquake sequence, *Geochem. Geophys. Geosyst.,* **6**(10), doi:10.1029/2005GC000935.

Geller, R., 1976. Scaling relations for earthquake source parameters and magnitudes, *Bull. seism. Soc. Am.,* **66,** 1501–1523.

Giovanni, M., Beck, S. & Wagner, L., 2002. The June 23, 2001 Peru earthquake and the Southern Peru subduction zone, *Geophys. Res. Lett.,* **29**(21), doi:10.1029/2002GL015774.

Given, J. & Helmberger, D., 1980. Upper mantle structure of Northwestern Eurasia, *J. geophys. Res.,* **85**(B12), 7183–7194.

Ishii, M., Shearer, P., Houston, H. & Vidale, J., 2005. Extent, duration, and speed of the 2004 Sumatra-Andaman earthquake imaged by the Hi-Net array, *Nature,* **435**(7044), 933–936, doi:10.1038/nature03675.

Kanamori, H., 1972. Mechanism of tsunami earthquakes, *Phys. Earth planet. Inter.,* **6,** 346–359.

Kanamori, H. & Rivera, L., 2008. Source inversion of *W* phase: speeding up seismic tsunami warning, *Geophys. J. Int.,* **175,** 222–238, doi:10.1111/j.1365-246X.2008.03887.x.

Kennett, B. (Ed.), 1991. *IASPEI 1991 Seismological Tables*, Research School of Earth Sciences, Australian National University, Canberra, Australia.

Kikuchi, M. & Kanamori, H., 1995. Source characteristics of the 1992 Nicaragua tsunami earthquake inferred from teleseismic body waves, *Pure appl. Geophys.,* **144**(3/4), 441–453.

Lander, J., Whiteside, L. & Lockridge, P., 2003. Two decades of global tsunamis, 1982-2002, *Int. J. Tsunami Soc.,* **21**(1), 3–82.

Lay, T., Kanamori, H., Ammon, C., Hutko, A., Furlong, K. & Rivera, L., 2009. The 2006-2007 Kuril islands great earthquake sequence, *J. geophys. Res.,* **114,** B11308, doi:10.1029/2008JB006280.

LeFevre, L. & Helmberger, D., 1989. Upper mantle *P* velocity structure of the Canadian shield, *J. geophys. Res.,* **94**(B12), 17 749–17 765.

López, A. & Okal, E., 2006. A seismological reassessment of the source of the 1946 Aleutian 'tsunami' earthquake, *Geophys. J. Int.,* **165**(3), 835–849, doi:10.1111/j.1365-246X.2006.02899.x.

MacInnes, B., Pinegina, T., Bourgeois, J., Razhigaeva, N., Kaistrenko, V. & Kravchunovskaya, E., 2009. Field survey and geological effects of the 15 November 2006 Kuril tsunami in the middle Kuril islands, *Pure appl. Geophys.,* **166,** 9–36, doi:10.1007/s00024-008-0428-3.

Newman, A. & Okal, E.A., 1998. Teleseismic estimates of radiated seismic energy: the E/M_0 discriminant for tsunami earthquakes, *J. geophys. Res.,* **103**(B11), 26 885–26 898.

Newman, A., Hayes, G., Wei, Y. & Convers, J., 2011. The 25 October 2010 Mentawai tsunami earthquake, from real-time discriminants, finite-fault rupture, and tsunami excitation, *Geophys. Res. Lett.,* **38,** L05302, doi:10.1029/2010GL046498.

Okal, E.A., 1992. A student's guide to teleseismic body wave amplitudes, *Seism. Res. Lett.,* **63**(2), 169–180.

Okal, E.A. & Talandier, J., 1989. M_m: a variable-period mantle magnitude, *J. geophys. Res.,* **94**(B4), 4169–4193.

Okal, E. *et al.*, 2002. Field survey of the Camaná, Perú tsunami of 23 June 2001, *Seism. Res. Lett.,* **73**(6), 907–920.

Park, S.-C. & Mori, J., 2007. Triggering of earthquakes during the 2000 Papua New Guinea earthquake sequence, *J. geophys. Res.,* **112,** B03302, doi:10.1029/2006JB004480.

Polet, J. & Kanamori, H., 2000. Shallow subduction zone earthquakes and their tsunamigenic potential, *Geophys. J. Int.,* **142,** 684–702.

Seno, T. & Hirata, K., 2007. Did the 2004 Sumatra-Andaman earthquake involve a component of tsunami earthquakes?, *Bull. seism. Soc. Am.,* **97**(1A), S296–S306, doi:10.1785/0120050615.

Stein, S. & Okal, E., 2005. Speed and size of the Sumatra earthquake, *Nature,* **434,** 581–582.

Stein, S. & Okal, E., 2007. Ultra-long-period seismic study of the December 2004 Indian Ocean earthquake and implications for regional tectonics and the subduction process, *Bull. seism. Soc. Am.,* **97**(1), S279–S295, doi:10.1785/0120050617.

Tanioka, Y., Ruff, L. & Satake, K., 1997. What controls the lateral variation of large earthquake occurrence along the Japan Trench?, *Island Arc,* **6,** 261–266.

Tolstoy, M. & Bohnenstiehl, D., 2005. Hydroacoustic constraints on the rupture duration, length, and speed of the great Sumatra-Andaman earthquake, *Seism. Res. Lett.,* **76,** 419–425.

Tregoning, P., Sambridge, M., McQueen, H., Toulmin, S. & Nicholson, T., 2005. Tectonic interpretation of aftershock relocations in eastern Papua New Guinea using teleseismic data and the arrival pattern method, *Geophys. J. Int.,* **160,** 1103–1111, doi:10.1111/j.1365-246X.2005.02567.x.

Tsai, V., Nettles, M., Ekström, G. & Dziewonski, A., 2005. Multiple CMT source analysis of the 2004 Sumatra earthquake, *Geophys. Res. Lett.,* **32,** L17304, doi:10.1029/2005GL023813.

Weinstein, S. & Okal, E.A., 2005. The mantle magnitude M_m and the slowness parameter Θ: five years of real-time use in the context of tsunami warning, *Bull. seism. Soc. Am.,* **95**(3), 779–799.

Wessel, P. & Smith, W., 1991. Free software helps map and display data, *EOS, Trans. Am. geophys. Un.,* **72**(41), 441, 445–446.